RSC Advances

REVIEW

View Article Online
View Journal | View Issue

Cite this: *RSC Adv.*, 2015, **5**, 40552

Heterogeneous Fenton catalysts for the abatement of organic pollutants from aqueous solution: a review

P. V. Nidheesh

Received 2nd February 2015
Accepted 13th April 2015

DOI: 10.1039/c5ra02023a

www.rsc.org/advances

Fenton processes have gained much attention in the field of wastewater treatment during recent years. In order to overcome the disadvantages of Fenton processes, research has focused more on the heterogeneous Fenton process, with highly active and stable solid catalysts. This review reports on advances in the field of heterogeneous Fenton processes in recent years, especially focusing on the various heterogeneous catalysts used. After a general introduction to the various Fenton processes, their advantages and the importance of heterogeneous Fenton processes, various catalysts used in heterogeneous Fenton processes are described in detail. These catalysts are divided into iron minerals, zero-valent iron, waste materials, iron- and iron oxide-loaded materials, and clay. The properties, stability, activity and pollutant degradation mechanism of various catalysts are also discussed in detail.

Introduction

The Fenton process is an advanced oxidation process (AOP), which uses ferrous ions and hydrogen peroxide for the generation of the second most powerful oxidant, *i.e.*, hydroxyl radicals in aqueous solution. Hydroxyl radicals produced *in situ* by the reaction between ferrous ions and hydrogen peroxide *via* the classical Fenton process (eqn (1)) destroy organic pollutants by redox reactions (eqn (2)), dehydrogenation (hydrogen abstraction) reactions (eqn (3)), and electrophilic addition to π systems (hydroxylation) (eqn (4)).[1,2] These reactions generate organic radicals and further oxidation reactions of these radicals with hydroxyl radicals result in complete mineralization of organic pollutants.

$$Fe^{2+} + H_2O_2 \rightarrow Fe^{3+} + OH^- + HO^{\bullet} \quad (1)$$

$$OH^{\bullet} + RX \rightarrow RX^{+\bullet} + OH^- \quad (2)$$

$$RH + OH^{\bullet} \rightarrow R^{\bullet} + H_2O \quad (3)$$

$$RHX + OH^{\bullet} \rightarrow RHX(OH) \quad (4)$$

Ferrous ions consumed during the Fenton reaction are regenerated by further reaction of ferric ions with hydrogen peroxide, as in eqn (5) and (6).[3,4]

$$Fe^{3+} + H_2O_2 \rightarrow Fe^{2+} + H^+ + HO_2^{\bullet} \quad (5)$$

$$Fe^{3+} + HO_2^{\bullet} \rightarrow Fe^{2+} + O_2 + H^+ \quad (6)$$

Department of Civil Engineering, National Institute of Technology, Calicut, Kerala, India. E-mail: nidheeshpv129@gmail.com

External energy in the form of UV light, electricity and ultrasound is added in the Fenton process to enhance its pollutant degradation efficiency. In general, Fenton processes can be classified as in Fig. 1.[5]

The electro Fenton (EF) process uses externally added ferrous ions and electrolytically produced hydrogen peroxide for the production of hydroxyl radicals. Hydrogen peroxide is produced near a cathode surface in acidic solution by two-electron reduction of oxygen, according to eqn (7).[1,6] Ferrous ions are regenerated by cathodic reduction of ferric ions in the EF process (eqn (8)), which increases the number of Fenton reaction cycles compared to conventional Fenton processes, due to the increased rate of ferrous ion regeneration compared to that in the conventional Fenton process.[7]

$$O_2 + 2H^+ + 2e^- \rightarrow H_2O_2 \quad (7)$$

$$Fe^{3+} + e^- \rightarrow Fe^{2+} \quad (8)$$

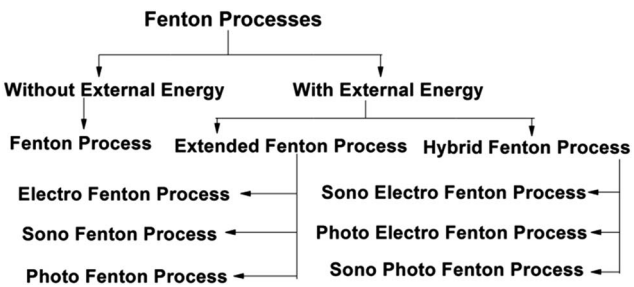

Fig. 1 Classification of Fenton processes. Figure taken from ref. 5.

A combination of UV irradiation and the Fenton process, known as the photo Fenton (PF) process, enhances the production of hydroxyl radicals by means of additional production of these radicals *via* UV decomposition of externally added hydrogen peroxide as in eqn (9).[8] The generation of ferrous ions from iron complexes in the presence of UV light also enhances the efficiency of the PF process compared to that of the conventional Fenton process.

$$H_2O_2 + h\nu \rightarrow 2HO^{\bullet} \quad (9)$$

In the case of the sono Fenton (SF) process, the presence of ultrasound irradiation produces a higher amount of hydroxyl radicals and other radicals in solution *via* acoustic cavitation phenomena. Hydroxyl radicals are produced in water *via* acoustic cavitation as in eqn (10).[9,10]

$$H_2O +))) \rightarrow HO^{\bullet} + H^{\bullet} \quad (10)$$

The advantages of the various Fenton processes are given in Table 1.

Even though there are so many advantages of the Fenton process, its practical application has been interrupted due to its disadvantages. The main disadvantage of the Fenton process is that its optimal catalytic activity is at pH 3. In many cases the pH of wastewater is either neutral or alkaline. Therefore, it is necessary to bring the solution pH to 3 for effective Fenton reactions.[32] The fact that the optimal pH of Fenton reactions is 3 is mainly due to the presence of higher concentrations of ferrous and ferric ions in solution compared to the case at other pH values. The pH of a solution has a significant effect on the solubility of metals. For example, a ferric ion added to a solution of pH 3 is in the form of $Fe(H_2O)_6^{3+}$.[3] This hexa-aqua ferric complex undergoes further hydrolysis and forms other complexes as in eqn (11) and (12).[4] The attraction between ligands and ferric ions in these complexes is higher than that between ferric ions and ligands in $Fe(H_2O)_6^{3+}$. An increase in pH from 3 increases the concentration of complexes other than $Fe(H_2O)_6^{3+}$. Therefore, the useful fraction of ferric ions for the Fenton process decreases with an increase in pH values.

$$[Fe(H_2O)_6]^{3+} + H_2O \rightarrow [Fe(H_2O)_5OH]^{2+} + H_3O^{+} \quad (11)$$

$$[Fe(H_2O)_5OH]^{2+} + H_2O \rightarrow [Fe(H_2O)_4(OH)_2]^{+} + H_3O^{+} \quad (12)$$

Another disadvantage of the Fenton process is the production of a higher amount of iron sludge. Due to the slow regeneration rate of ferrous ions in the Fenton process, the amount of ferric ions increases with the reaction time. This increased concentration of ferric ions results in formation of insoluble complexes. Also, the concentration of hydroxyl ions increases with Fenton reactions. This also increases the pH of the solution and results in further production of iron sludge. Therefore, additional downstream treatment of the generated sludge is required in the conventional Fenton process. The removal of pollutants in the classical Fenton process is a combination of degradation and separation processes. The rate of sludge production can be decreased by increasing the regeneration rate of ferrous ions and stabilizing the pH at 3. The addition of external energy to the conventional Fenton process increases the regeneration rate of ferrous ions. However, the solution pH is maintained at 3 only in the electro Fenton process by water oxidation at the anode as in eqn (13).[33]

$$2H_2O \rightarrow O_2 + 4H^{+} + 4e^{-} \quad (13)$$

In order to overcome the disadvantages of Fenton processes, research has focused more on heterogeneous Fenton processes. A solid catalyst is used as a source of iron in heterogeneous Fenton processes instead of ferrous ions in homogeneous Fenton processes. With the use of a heterogeneous Fenton process, the rate of sludge production can be regulated. This sludge production mainly depends on the metal-leaching properties of heterogeneous catalysts and increases with an increase in the leaching rate. Generally, leaching of metal ions from the catalyst is very slight and results in insignificant sludge

Table 1 Advantages of Fenton processes

Process	Advantages	References
Fenton	• Short reaction time • Highly complicated apparatus and pressurized systems are not required • Catalysts are economic and non-toxic • No energy input is required to activate H_2O_2	11–13
Electro Fenton	• Electrolytic generation of hydrogen peroxide • Regeneration of ferrous ions *via* cathodic reduction of ferric ions • Absence of harmful reagents • Environment-friendly method • Absence of sludge production • Insignificant change in solution pH, which results in degradation as a more dominant pollutant removal mechanism than separation	1, 2 and 14–27
Photo Fenton	• Additional generation of hydroxyl radicals by decomposition of hydrogen peroxide • Rapid regeneration of ferrous ions in the presence of UV light • Iron sludge formation is very slight compared to conventional Fenton process	8–10 and 28
Sono Fenton	• Additional generation of hydroxyl radicals from water and oxygen • Enhanced regeneration rate of ferrous ions • Potential for H_2O_2 production of ultrasonic irradiation	29–31

generation. Therefore, further sludge treatment, as in a homogeneous Fenton process, is not required for a heterogeneous Fenton process. In the case of a homogeneous Fenton process, the amount of ferrous ions consumed increases with the reaction time. In a heterogeneous Fenton process, the amount of iron species consumed is less, due to very low leaching properties. After the Fenton process, the catalysts are easily separable.

In a homogeneous Fenton process, the source of hydroxyl radical generation is externally added ferrous ions. In the case of a heterogeneous Fenton process, the catalyst contains surface ferrous and ferric ions. These ions serve as a source of hydroxyl radical production. Most heterogeneous Fenton catalysts used are porous materials. Due to their porous nature, pollutants may be adsorbed on the surface of the catalyst. This sorption of pollutants increases the rate of pollutant degradation in heterogeneous Fenton processes. Recycling of the catalyst is another advantage of heterogeneous Fenton processes over homogeneous Fenton processes. Most of the catalysts studied are more stable even after multiple uses. The main disadvantage of a homogeneous Fenton process is its narrow pH range. However, results show that most heterogeneous catalysts are efficient in a wide range of pH values.

Various types of heterogeneous catalysts are used for the degradation of organic pollutants *via* Fenton oxidation (Fig. 2). Different iron oxides such as ferrihydrite, hematite, goethite, lepidocrocite, magnetite, pyrite, *etc.* have been used as efficient Fenton catalysts for the abatement of various organic pollutants. Soil, including clay and laterite, and industrial waste containing iron such as fly ash, pyrite ash, blast furnace dust, electric arc furnace dust, *etc.* are also used as sources of iron species in the Fenton reaction. Other research has focused on the immobilization of iron compounds on different supports. The supports used for immobilization of iron are mostly porous in nature. Various materials such as clay, activated carbon, alumina, silica, zeolite, fibers, biosorbents, hydrogels, *etc.* are used as efficient supports for iron and iron oxides.

This review focuses on the various heterogeneous Fenton catalysts used for the degradation of organic pollutants. The paper is organized by subdividing the materials into iron minerals, zero-valent iron, soils, iron- and iron oxide-loaded materials and waste materials. These materials are also categorized based on their properties. The properties of the materials used, their preparation methods and Fenton catalytic efficiencies are also explained. Special attention is paid to leaching, pollutant degradation mechanisms and the reusability of heterogeneous catalysts.

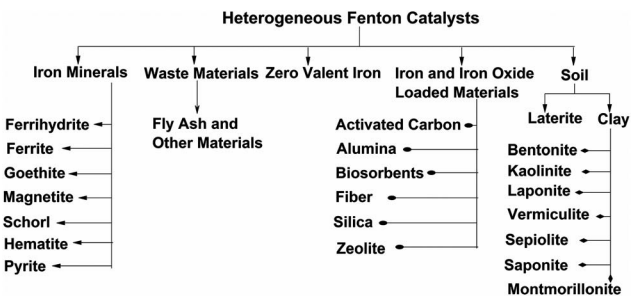

Fig. 2 Classification of heterogeneous Fenton catalysts.

Heterogeneous Fenton catalysts

Iron minerals

Due to their strong adsorption capacity, low cost, easy separation, natural abundance, environment-friendly properties and enhanced stability, iron oxides have received much attention for removing heavy metals and organic pollutants from wastewater.[34] A variety of iron minerals are used as heterogeneous Fenton catalysts for the mineralization of various persistent organic pollutants. The application of iron minerals as Fenton catalysts has the following advantages:[35] (1) the effluent pH may be in the range of 5 to 9; (2) catalyst removal after treatment is very easy; (3) long catalyst lifetime; and (4) insignificant effect of inorganic carbonates on the reactions. However, the main disadvantage of heterogeneous Fenton processes using iron minerals is the slower degradation rate of organic pollutants compared to the classical Fenton process.[36] This disadvantage can be regulated by the addition of chelating compounds such as citrate, malonate, ethylenediaminetetraacetic acid and oxalate. For example, Huang *et al.*[36] used ethylenediamine-*N*,*N*′-disuccinic acid as a chelating compound during degradation of bisphenol A. The following are the main types of minerals used as heterogeneous Fenton catalysts.

Ferrihydrite

Ferrihydrite is a naturally occurring hydrous ferric oxyhydroxide and exists in the earth's crust in great quantities.[37,38] During the preparation of goethite and hematite, ferrihydrite is used as a precursor.[39] The specific surface area of ferrihydrite is in the range of 250–275 $m^2\ g^{-1}$.[37] Its large surface area and reactivity help ferrihydrite to serve as a dominant sink for various metals and nutrients.[40] In the Fenton system, this higher surface area increases contact between ferrihydrite and hydrogen peroxide, which results in higher removal efficiency. Under UV radiation, iron species were dissolved from ferrihydrite in the form of $Fe(OH)^{2+}$ and $Fe(OH)_2^{+}$.[40] These soluble ferric hydroxides are responsible for further Fenton reactions. The properties and catalytic activity of ferrihydrite are summarized in Table 2.

Ferrite

Ferrites are ceramic compounds formed by combination of iron oxides with other transition metals.[42] According to their crystal structures, ferrites are classified as garnet, hexagonal and spinel ferrites. Among these, spinel ferrites have received much interest as heterogeneous Fenton catalysts for the removal of various organic pollutants. Spinel ferrites have a face-centred cubic lattice with a general formula of $M_xFe_{3-x}O_4$ (where M represents one or more bivalent metal ions such as Zn, Mn, Co, *etc.*), in which oxide ions are arranged in a face-centred cubic manner and metal ions are arranged at tetrahedral and octahedral sites.[43] The preparation methods, properties and Fenton catalytic activity of ferrite are given in Table 3. Among these

Table 2 Properties and catalytic activity of ferrihydrite

Pollutant	Catalyst preparation method	Properties of catalyst	Process	Major findings	Optimal operating conditions and removal efficiency	Reference
Atrazine	—	Specific surface area 42 $m^2 g^{-1}$	Fenton process	• A higher decomposition rate of hydrogen peroxide at pH 8 than at pH 3 • The authors suggested two mechanisms for oxidation of the pollutant in the presence of a ferrihydrite catalyst • At lower pH values, the degradation of pollutants is mainly due to Fenton reactions occurring in solution *via* dissolved iron species from the heterogeneous catalyst • Non-reactive oxygen species were produced at higher pH values by ferrihydrite surface decomposition of hydrogen peroxide	Atrazine degradation rate is 0.5 per day at [atrazine] = 37 μM, $[H_2O_2]$ = 2 mM, [ferrihydrite] = 0.2 g L^{-1}, $[Na_2SO_4]$ = 10 mM, pH 3.0	Barreiro *et al.*[41]
Mordant yellow 10	Precipitation followed by thermal treatment at 40 °C		Photo Fenton process	• Increased catalytic performance of ferrihydrite with a decrease in solution pH	• More than 90% mordant yellow 10 degradation • 0.5 g L^{-1} ferrihydrite, 3 mM H_2O_2 and temperatures of 288–318 K are found to be highly photoactive conditions for dye degradation	Wang *et al.*[38]
P-Nitrophenol	Precipitation followed by thermal treatment at 40 °C	• Molecular formula of the material is $5Fe_2O_3 \cdot 8H_2O$ • Mesoporous structure • Sample exhibits type III isotherm • Total and external surface areas were 228.83 and 158.97 $m^2 g^{-1}$, respectively • Mean pore size and total pore area were 16.38 nm and 69.85 $m^2 g^{-1}$	Photo Fenton process	Suggested a ferrihydrite to hydrogen peroxide molar ratio of 1 : 0.225 as an optimal condition for the degradation of *p*-nitrophenol	More than 94.5% pollutant removal at $[H_2O_2]$ = 0.45 mM, [catalyst] = 0.2 g L^{-1}, pH 3 and time 5 h	Wu *et al.*[40]

Table 2 (*Contd.*)

Pollutant	Catalyst preparation method	Properties of catalyst	Process	Major findings	Optimal operating conditions and removal efficiency	Reference
Methylene blue	Precipitation followed by thermal treatment at 60 °C for 24 h	• In XRD analysis, two broad peaks at 35° and 63° were found • Sample exhibits type IV isotherm • Flower-like ferrihydrite has pores with diameters of *ca.* 18 nm And BET surface area is 276.2 $m^2 g^{-1}$ • The product obtained in the absence of citrate is made of a mixture of goethite and magnetite	Photo Fenton process	• Observed significant changes in the surface properties and adsorption ability of ferrihydrite *via* modification with citrate • Fenton reactions were enhanced by the presence of surface ferrous ions	99.7% dye removal within 120 min under visible light	Zhang *et al.*[34]

catalysts, Mn-substituted cobalt ferrites have higher catalytic efficiency for degradation of both anionic and cationic dyes.[43] More than 90% dye degradation was observed by researchers within a time period of 40–90 min in the dark and within 20–30 min under visible-light irradiation.

Goethite

Goethite is an iron oxyhydroxide, which is found in soil and other low-temperature environments.[49] The main component of rust and bog iron ore is goethite. Among iron oxides, goethite is used more commonly as a heterogeneous catalyst due to the fact that it is:[50] (1) one of the most common forms of iron oxide, (2) a very environmentally friendly catalyst, (3) one of the most chemically active compounds suspended in natural water, (4) cheap, and it has (5) very high thermodynamic stability and (6) a low energy requirement. Muruganandham *et al.*[51] used goethite as a heterogeneous sono Fenton catalyst for the degradation of direct orange 39 dye from aqueous solution and observed more than 80% dye removal after 90 min of sonication. Similarly, complete removal of bisphenol A was observed by Huang *et al.*[36] in the presence of a goethite catalyst, ethylenediamine-*N*,*N*′-disuccinic acid chelating agent and UV radiation at near-neutral pH. Goethite also exhibits higher efficiency for removing 2-chlorophenol[52–54] and picric acid[55] from aqueous solution.

Ortiz de la Plata *et al.*[50] studied the optical properties of a goethite catalyst by analyzing its specific absorption coefficients, specific scattering coefficients, and the asymmetry factor for the Henyey–Greenstein phase function and found values between 310 and 500 nm. From these results, the authors concluded that this catalyst is very suitable for the photo Fenton process in the presence of solar radiation.

Schorl

Schorl is the most common form of tourmaline and is known as "Black Tourmaline", because it is one of the most ornamental black minerals known.[56] Tourmaline is a crystalline borosilicate mineral compounded with elements such as aluminium, iron, magnesium, sodium, lithium or potassium.[57] The general formula of tourmaline may be written as $XY_3Z_6[Si_6O_{18}][BO_3]W_4$, where X = Ca, Na, K or vacancy; Y = Li, Mg, Fe^{2+}, Mn^{2+}, Al, Cr^{3+}, V^{3+}, Fe^{3+}; Z = Mg, Al, Fe^{3+}, V^{3+}, Cr^{3+}; and W = OH, F, O.[58] Among these minerals, schorl (chemical formula: $NaFe_3^{2+}Al_6(BO_3)_3$-$Si_6O_{18}(OH)_4$) has unique characteristics of pyroelectricity and piezoelectricity.[59] Experimental results have proved that schorl is an efficient heterogeneous Fenton catalyst for the oxidation of various organic pollutants. Xu *et al.*[60] used schorl for the abatement of argazol blue dye and observed complete decolorization within 4 min and 72% mineralization within 200 min. Similar results have been reported for the degradation of rhodamine B *via* heterogeneous Fenton oxidation.[61] Xu *et al.*[62] used schorl sintered at various temperatures ranging from 750 °C to 1050 °C for the oxidation of methyl orange and observed a decrease in its removal efficiency with the sintering process. This is mainly due to the complete disappearance of schorl crystals with the sintering process and the appearance of hematite and spinel on the surface of the catalyst. These

Table 3 Properties and catalytic activity of ferrite

Catalyst	Pollutant	Catalyst preparation method	Properties of catalyst	Process	Major findings	Optimal operating conditions and removal efficiency	Reference
Nickel ferrite	Rhodamine B	Precipitation followed by thermal treatment at 180 °C for 10 h and sintering at 200 °C for 4 h	Synthesized samples were significantly broader than the bulk sample. Average diameter of particles was 8.9 nm. Specific area of 73.14 $m^2 g^{-1}$. The coercivity was 29.37 Oe and the saturation magnetization was 40.38 emu g^{-1}	Photo Fenton process	The authors recognized nickel ferrite as a very stable, recoverable, highly active, and easily separable heterogeneous Fenton catalyst	COD removal of 83% and TOC removal of 49% were observed after dye oxidation using 4 g L^{-1} catalyst and after 3 h contact time	Liu *et al.*[44]
Bismuth ferrite	Phenol	Precipitation followed by thermal treatment at 400 °C for 30 min	Impure nanoparticles exhibited higher magnetization than pure nanoparticles. The materials exhibit strong photo-absorption in the visible-light region	Fenton and photo Fenton processes	Complete degradation of phenol and its derivatives such as 4-chlorophenol, 2,4,6-trichlorophenol, biphenyl, 4-nitrophenol, 2,4-dinitrophenol and 2,4,6-trinitrophenol	Complete degradation of phenolic. Compounds was achieved under solar light irradiation with 0.06 g catalyst, pH 2.5 and 0.8 mM H_2O_2	Soltani and Entezari[45]
Mesoporous silica encapsulated with magnetic $MnFe_2O_4$	Methyl orange	Solvothermal method	$MnFe_2O_4$ nanoparticles are spherical in shape having a mean diameter of 90–100 nm. Mesoporous silica encapsulated with magnetic $MnFe_2O_4$ is monodisperse with a mean diameter of 200 nm and a surface area of 423 $m^2 g^{-1}$. Nanoparticles are superparamagnetic in nature at room temperature	Fenton process	Enhanced efficiency of the prepared catalyst was observed in the presence of ultrasound radiation and photolysis under sunlight. The degradation phenomenon could be attributed to the porous structure of the catalyst which adsorbs dye molecules followed by decolourisation by central magnetic $MnFe_2O_4$ nanoparticles	More than 90% degradation for a dye with initial concentration of 0.6 mg mL^{-1} at pH 2, 2 mL 30% H_2O_2, 20 mg catalyst and temperature 28 °C	Sahoo *et al.*[46]
Transition metal-substituted cobalt nanoferrites	—	Precipitation followed by thermal treatment at 90 °C and annealing in a muffle furnace for 2 h	Spherical morphology of particles. With an increase in annealing temperature from 400 °C to 1000 °C, the average particle size is increased from 20 nm to 60 nm. All the ferrite compositions crystallize in a cubic spinel structure	Fenton process	The catalytic activity is largely dependent on the cation distribution and the presence of oxygen vacancies on the surface of the ferrite catalyst. In the case of cobalt ferrites, the rate of Fenton reactions slows down with the annealing temperature. The rate of Fenton activity follows the order $CoCrFeO_4$ > $CoCr_{0.8}Fe_{1.2}O_4$ > $CoCr_{0.6}Fe_{1.4}O_4$ > $CoCr_{0.2}Fe_{1.8}O_4$ > $CoCr_{0.4}Fe_{1.6}O_4$	—	Jauhar and Singhal[47]
Nickel-doped cobalt ferrite	Rhodamine B and 4-nitrophenol	Reverse micelle method	The particles are spherical with an ordered cubic spinel structure and have a crystallite size of 4–6 nm. Surface area of 152 $m^2 g^{-1}$	Photo Fenton process	$Co_{0.4}Ni_{0.6}Fe_2O_4$ exhibited the best catalytic activity for the reduction of 4-nitrophenol to 4-aminophenol in the presence of $NaBH_4$ as reducing agent. $CoFe_2O_4$ was found to be catalytically inactive. 99% rhodamine B degradation in the presence of nickel-doped cobalt ferrite nanoparticles was observed	97% dye degradation in 90 min for 50 mg nickel cobalt ferrite nanoparticles and 100 μL 30% H_2O_2 at a pH of 2	Singh *et al.*[48]

Table 4 Properties and catalytic activity of hematite

Catalyst	Pollutant	Catalyst preparation method	Properties of catalyst	Process	Major findings	Optimal operating conditions and removal efficiency	Reference
Nb-containing hematites	Methylene blue	Co-precipitation method	• Surface area increased with an increase in Nb concentration which was mainly due to a decrease in particle size and a decrease in pore diameter	Fenton process	• Catalyst is less active only in the presence of UV light	70% color removal and 25% mineralization in the presence of 10 mg catalyst, 0.3 mol L^{-1} H_2O_2 at pH 6	Silva *et al.*[66]
Nb-doped hematite	Methylene blue	Emulsion method	• Surface area increased with Nb addition	Fenton process	• No niobium oxide formation in the catalyst • The use of templates in the synthesis of oxides promoted the production of very homogeneous material and small spherical particle size • Doping with niobium can promote lower dispersion and a reduction in particle size	75% dye removal in the presence of 10 mg catalyst and 8 mol L^{-1} H_2O_2 at pH 5.5	Oliveira *et al.*[67]
Cu-doped hematite	Coomassie brilliant blue R 250	Co-precipitation followed by thermal treatment at 400 °C for 2 h	• Loading with copper increased the surface area of the catalyst • Negligible amount of copper leaching from the catalyst	Photo Fenton process	• Loading with copper leads to the formation of smaller and more regular particles • An enhancement in the degradation rate of the dye from 2.16×10^{-4} s^{-1} to 3.07×10^{-4} s^{-1} was observed with doping of copper in hematite	63% COD removal with a dye degradation rate of 3.07×10^{-4} s^{-1} in optimal conditions	Ameta *et al.*[68]
Fe@Fe_2O_3 core–shell nanowires	Rhodamine B	Precipitation method	—	Fenton process	• Fe@Fe_2O_3 core–shell nanowires enhanced the conventional Fenton oxidation of dye molecules by the generation of superoxide radicals *via* activation of molecular oxygen induced by Fe@Fe_2O_3 core–shell nanowires • Generation of hydroxyl radicals in the presence of Fe@Fe_2O_3 core–shell nanowires in the Fenton process is 38 times higher than that of ferrous ions	80% dye degradation in 30 min at an initial pH of 4.3, $[Fe^{2+}] = 5 \times 10^{-5}$ mol L^{-1}, $[H_2O_2] = 8 \times 10^{-5}$ mol L^{-1} and $[Fe@Fe_2O_3] = 0.2$ g L^{-1}	Shi *et al.*[69]
S-doped hematite	Acid orange 7 and phenol	Hybrid hydrothermal-calcination method	• Short rod-like particles • S element was doped in the forms of FeS or FeS_2	Photo Fenton	• Catalyst Exhibited little Fenton reactivity in the dark • Particle Displays excellent Fenton activity under either UV or visible irradiation • S doping enhanced the photo Fenton activity of the catalyst by retarding recombination of photogenerated charge carriers and promoting electron transfer between peroxide species and iron ions at the interface	Almost complete removal of dye and 90% phenol removal in the presence of 0.1 g L^{-1} catalyst	Guo *et al.*[70]

Table 4 (*Contd.*)

Catalyst	Pollutant	Catalyst preparation method	Properties of catalyst	Process	Major findings	Optimal operating conditions and removal efficiency	Reference
S,N-co-doped hematite	Rhodamine B	Co-precipitation technique	• Diameters of the particles lie in the range of 20–40 nm • Particles Exhibit a type IV nitrogen sorption isotherm • Surface areas are in the range of 13–57 $m^2 g^{-1}$ • Pore volume is in the range of 0.1–0.34 $cm^3 g^{-1}$	Photo Fenton	• The introduction of strong diffraction along the [110] plane is a determining factor for the enhancement in the photo Fenton activity of hematite with doping of sulphur • Higher catalytic activity for S,N-co-doped hematite compared to that of hematite was observed with doping by individual elements • Both sulphur and nitrogen control electron–hole recombination by creating trap states	95% dye degradation after 4 h natural sunlight illumination and in the presence of 20 mg catalyst and 0.1 mmol hydrogen peroxide	Pradhan *et al.*[71]

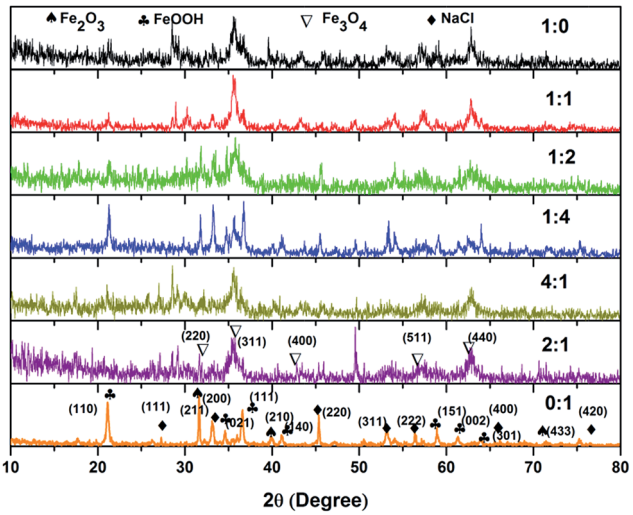

Fig. 3 XRD spectra of magnetite prepared with various ferrous-to-ferric ion ratios. Taken from Ref. 80.

changes in mineral composition result in disappearance of the spontaneous 'electrostatic poles' on the surface of a schorl crystal, which leads to decreased attractive force between schorl and methyl orange and lower removal efficiency.

Hematite

Hematite is a principal ore of iron that exists in various types such as kidney ore, martite, iron rose and specularite; it is colored black to steel or silver-grey, brown to reddish-brown, or red.[63] Hematite has received much attention as a heterogeneous catalyst due to the fact that it is:[64,65] (1) a low-cost abundant mineral, and it has (2) large surface area, (3) high surface-to-volume ratio, (4) particular morphology, (5) well-defined topology, and (6) even after losing its reactivity, it can be used as a feed material for pig iron production in a blast furnace without having any environmental impact. In optimal conditions, hematite has the ability to remove more than 99% of a dye from aqueous solution after 120 min of contact time.[64,65] Doping of other heavy metal and non-metal ions in hematite also increased its pollutant degradation ability. The properties and catalytic activity of hematite are given in Table 4.

Magnetite

Magnetite is a mixed-valence iron oxide and a member of the spinel group having unique redox properties.[72] Among all the naturally occurring minerals on Earth, magnetite is the most magnetic.[73] Magnetite has received considerable interest in heterogeneous Fenton systems due to its structural ferrous ions, which play an important role in the initiation of the Fenton reaction according to the classical Haber–Weiss mechanism.[74,75] In addition to this, magnetite particles can be easily separated after purification processes from an aqueous medium by means of magnetic separation.[76] Also, magnetite is able to function steadily as a heterogeneous catalyst without substantial loss of mass.[77] Recent studies indicated that magnetite is an efficient heterogeneous Fenton catalyst for the abatement of various

persistent organic pollutants. Sun and Lemley[72] used magnetite as a heterogeneous Fenton catalyst for the degradation of *p*-nitrophenol and observed 90% degradation of the pollutant after 10 h in optimal conditions. Pastrana-Martínez *et al.*[78] synthesized magnetite by a solvothermal method under alkaline conditions and used it as an effective heterogeneous photo Fenton catalyst for the oxidation of diphenhydramine. The authors observed complete removal of the pollutant from water, even at low catalyst concentrations. He *et al.*[79] synthesized magnetite having a surface area of 57.84 $m^2 g^{-1}$ and tested its Fenton activity for the degradation of catechol and 4-chlorocatechol. The authors observed 40% mineralization of pollutants from aqueous solution in the presence of a magnetite catalyst. Nidheesh *et al.*[80] prepared magnetite with various ferrous-to-ferric ion ratios by a chemical precipitation method and observed that magnetite with a 2 : 1 ratio exhibits higher Fenton catalytic activity for rhodamine B degradation. XRD patterns of magnetite prepared with various ferrous-to-ferric ratios are shown in Fig. 3. The crystallinity and particle size of the material increased with an increase in ferric ion concentration. Magnetite prepared only with ferric ions was crystalline in nature and did not form any black precipitate of magnetite. That particle was composed of NaCl, $NaOCl_2$, FeOOH and Fe_2O_3. In optimal conditions, more than 97% of the dye was removed after 180 min of electrolysis. A similar material was used by Xavier *et al.*[81] for Fenton oxidation of reactive dye magenta MB. The authors compared the efficiencies of homogeneous and heterogeneous Fenton processes and found similar efficiency for both processes.

Doping of heavy metals in magnetite also enhanced its catalytic efficiency. Compared to chromium-doped magnetite, vanadium-doped magnetite displayed higher efficiency for pollutant degradation.[82] Doping of vanadium increases the

Table 5 Properties and catalytic activity of pyrite

Pollutant	Catalyst preparation method	Properties of catalyst	Process	Major findings	Optimal operating conditions and removal efficiency	Reference
Trichloroethylene	Commercially available	—	Fenton process	• A heterogeneous Fenton process using pyrite is more effective and durable than the conventional Fenton reaction for the degradation of trichloroethylene	Almost complete removal of pollutant at [pyrite] = 2.14 g L^{-1}, and $[H_2O_2]$ = 251 mM	Che *et al.*[90]
Diclofenac	Commercially available	—	Fenton process	• Complete degradation of pollutant occurred in the presence of the heterogeneous catalyst, whereas the efficiency of a conventional Fenton process was only 65% • Continuous dissolution of ferrous ions from the catalyst surface is the key factor for the complete degradation of the pollutant	Complete removal of contaminant at [pyrite] = 0.5 mM and $[H_2O_2]$ = 1.0 mM	Bae *et al.*[91]
Nitrobenzene	Commercially available	Non-uniform shape of micro-sized particles, iron content of 24.67%, Surface area of 3.989 $m^2 g^{-1}$	Fenton process	• The initial pH has little effect on nitrobenzene degradation • Continuous dissolution of ferrous ions from the catalyst surface is the key factor for pollutant degradation	80% pollutant degradation at [pyrite] = 2 g L^{-1} and $[H_2O_2]$ = 250 mM	Zhang *et al.*[92]
Pyrene in soil washing, wastewater aided by cetylpyridinium chloride	Commercially available	—	Fenton process	• Higher degradation of pollutant in heterogeneous Fenton process than in conventional Fenton process	96% pollutant degradation at 25 mM pyrite, 9.8 mM H_2O_2 and initial pH 7	Choi *et al.*[93]
Reactive black 5, acid red GR, and cationic, red X-GRL	Commercially available	Iron content 39%, surface area of 2 $m^2 g^{-1}$	Fenton process	• Higher amount of iron and sulphate leaching from natural pyrite during the reaction • Iron leached from pyrite is responsible for the dye degradation	85% reactive black 5 and acid red GR removal within 10 min in the presence of 0.3 mM H_2O_2 and 0.3 g L^{-1} pyrite at initial pH values ranging from 6.3 to 6.9	Wu *et al.*[94]

concentration of ferric ions and the specific surface area of magnetite particles. Liang *et al.*[83] found an increase in surface hydroxyl groups and a decrease in the temperature of the maghemite to hematite phase transformation with the incorporation of vanadium in magnetite. The authors also observed higher catalytic activity of the heterogeneous catalyst, which was mainly due to improved adsorption activity, intensification of decomposition of H_2O_2 by vanadium on the magnetite surface to produce hydroxyl radicals, and enhanced regeneration of ferrous ions owing to improved electron transfer by vanadium. Similarly, doping of Ti,[84] Pd,[85] Nb,[86] *etc.* also enhanced the catalytic activity of magnetite. Zhong *et al.*[87] compared the enhancement in the Fenton and photo Fenton activities of magnetite with the addition of Ti, Cr, Mn, Co and Ni. In heterogeneous Fenton reactions, substitutions by Cr, Mn and Co enhanced the activity of magnetite by increasing the rate of formation of hydroxyl radicals. However, the addition of Ni and Ti in magnetite showed a negative effect. The addition of Ti, Mn and Cr enhanced the photo Fenton activity of magnetite, whereas an insignificant change was observed with the addition of Ni and Co.

Pyrite

The mineral pyrite, or iron pyrite, is an iron sulphide with the formula FeS_2 and is commonly known as fool's gold.[88] It is the most abundant metal sulphide on Earth and is known to spontaneously form hydrogen peroxide when exposed to water.[89] Formation of hydrogen peroxide in pyrite slurries may occur in two ways: (1) reaction of dissolved oxygen with leached ferrous ions and (2) reaction of dissolved oxygen with ferrous ions on the surface of pyrite. Surface bound or dissolved ferrous ions react with dissolved oxygen *via* the Haber–Weiss reaction mechanism and form hydrogen peroxide (eqn (14) and (15)) with superoxide as an intermediate species.[89] Formation of hydrogen peroxide also enhances the oxidation of organic pollutants.

$$Fe^{2+} + O_2 \rightarrow Fe^{3+} + O_2^{\cdot -} \quad (14)$$

$$Fe^{2+} + O_2^{\cdot -} + 2H^+ \rightarrow H_2O_2 + Fe^{3+} \quad (15)$$

Pyrite has been successfully used as a heterogeneous Fenton catalyst for the oxidative degradation of various organic contaminants. The properties and catalytic activity of pyrite are given in Table 5. Transformation of lactate into pyruvate in the presence of pyrite and the absence of hydrogen peroxide was observed by Wang *et al.*[95] This result also indicates that pyrite can generate both hydrogen peroxide and hydroxyl radicals in an aqueous medium. In addition, Fenton systems with pyrite overcome the major disadvantages of conventional Fenton processes such as termination of the Fenton reaction and the need to maintain an acidic pH environment.[92]

Zero-valent iron

In recent years, zero-valent iron (ZVI) has received much attention in the area of water and wastewater treatment techniques. Due to its low cost, efficiency and accessibility, ZVI is a very promising reactive medium for the abatement of various contaminants.[96] ZVI can be synthesized by various chemical methods such as chemical vapour deposition, spark discharge generation, thermal reduction of oxide compounds, hydrogenation of metallic complexes, pulsed laser ablation, thermal decomposition, sputtering gas aggregation, inert gas condensation and aqueous reduction of iron salts.[97] ZVI exhibits a dual surface property in which the core is covered with iron and the shell with iron oxides.[98] This dual property helps it to act as an efficient catalyst for the removal of various pollutants from water and wastewater.

ZVI is also a well-known Fenton catalyst. With the addition of hydrogen peroxide, ZVI reacts with hydrogen peroxide and forms ferrous ions in solution, as in eqn (16).[99] These ferrous ions undergo further Fenton reaction and produce hydroxyl radicals in the system.

$$H_2O_2 + Fe^0 \rightarrow Fe^{2+} + 2OH^- \quad (16)$$

Degradation of two surfactants, namely sodium dodecylbenzene sulfonate (DBS) and dodecylpyridinium chloride (DPC), using heterogeneous Fenton and sono Fenton processes in the presence of ZVI was studied by Naldoni *et al.*[100] The authors observed 51% mineralization of DBS by a heterogeneous Fenton process and the addition of ultrasound to this system increased the process efficiency to 93%. In the same conditions, 87% of DPC was mineralized. Min *et al.*[101] compared the efficiencies of un-annealed and annealed ZVI for the abatement of the fungicide tolclofos-methyl and found that un-annealed ZVI displays higher catalytic performance than that of annealed ZVI. The authors also observed an enhancement in the catalytic activity of ZVI with the addition of salts and observed the order of enhancement to be: $FeCl_3 > Fe_2(SO_4)_3 > FeSO_4 > Al_2(SO_4)_3$. Taha and Ibrahim[102] optimized COD removal from anaerobically treated palm oil mill effluent using an aerated Fenton process in the presence of ZVI as catalyst and found that 75% of COD could be removed from wastewater in optimal conditions such as: ZVI concentration of 3.9 g L^{-1}, hydrogen peroxide concentration of 1.8 g L^{-1} and 240 min of aeration. Similarly, a heterogeneous Fenton process has the ability to degrade 60 mg L^{-1} *p*-chloronitrobenzene in optimal conditions such as 268.8 mg L^{-1} ZVI and 4.9 mmol L^{-1} hydrogen peroxide with a contact time of 30 min.[103] Zha *et al.*[104] used ZVI for the abatement of amoxicillin and observed 86.5% pollutant degradation and 71.2% COD removal.

An important property of iron nanoparticles is their ability to reduce metal ions having higher standard electrode potentials than that of iron.[105] Yin *et al.*[106] used this property for removing

Table 6 Changes in characteristics of FA based on source[109]

Component	Bituminous	Sub-bituminous	Lignite
SiO_2 (%)	20–60	40–60	15–45
Al_2O_3 (%)	5–35	20–30	20–25
Fe_2O_3 (%)	10–40	4–10	4–15
CaO (%)	1–12	5–30	15–40
Loss on ignition (%)	0–15	0–3	0–5

Cr^{4+} and 4-chlorophenol simultaneously from an aqueous medium. Cr^{4+} was removed by reduction in the presence of ZVI followed by co-precipitation with ferric ions. Cr^{3+} was formed *via* reduction of Cr^{4+} and forms complexes such as $FeCr_2O_4$ and $Cr_xFe_{1-x}(OH)_3$ with ferric ions. 4-Chlorophenol was removed by Fenton reactions. In the optimal conditions, 100% pollutant removal and 37% TOC removal were observed by the authors.

In order to evaluate the effectiveness of a heterogeneous Fenton process using ZVI, Yu *et al.*[107] observed the changes in oxidation–reduction potential, pH and dissolved oxygen during the oxidation of synthetic textile wastewater. The authors observed a direct and meaningful relation between the changes in oxidation–reduction potential, pH and dissolved oxygen during Fenton reactions and the color and COD removal efficiencies of the system. They suggested that oxidation–reduction potential, pH and dissolved oxygen values can be used as criteria to determine the removal efficiency of a heterogeneous Fenton system using ZVI as catalyst.

Waste materials

Fly ash. Fly ash (FA) is an industrial by-product produced after the combustion process and contains fine particles, which rise with flue gas. Although FA is a good adsorbent for the removal of heavy metals,[108] efficient disposal of fly ash is a global issue. The mineral composition of FA varies with its source. The characteristics of FA produced from various sources are given in Table 6.

From the table, it can be seen that FA contains significant amounts of iron species and can be used as an efficient Fenton catalyst. FA has a high specific area in the range of 0.4 $m^2\ g^{-1}$.[108] Fly ash can be used as a catalyst and catalyst support due to the high stability of its major component, aluminosilicates.[110] Chen and Du[111] used fly ash as an efficient heterogeneous Fenton catalyst for the degradation of *n*-butyl xanthate and observed ~97% pollutant degradation, even though the iron oxide concentration in the fly ash was in the range of 4%. Song and Li[112] observed higher dye degradation efficiency with FA as compared to kaolinite and diatomaceous earth. A sono Fenton process using FA had the ability to degrade 99% of direct black 168 from aqueous solution at the optimal FA concentration of 2 g L^{-1}. In a similar way, Li *et al.*[113] observed 96% acid orange degradation *via* a sono Fenton process using 2.5 g L^{-1} FA.

Modified FA is also a good heterogeneous Fenton catalyst for the abatement of various persistent organic pollutants. Duc[114] studied the degradation of reactive blue 181 using FA loaded with iron and reported that 87% of the dye was removed effectively at the optimal catalyst concentration of 0.4 g L^{-1}. Zhang *et al.*[115] used FA activated with nitric acid for the abatement of *p*-nitrophenol from aqueous solution. By this activation process, the SiO_2 and Fe_2O_3 concentrations of fly ash increased, while those of CaO and Al_2O_3 decreased in a significant manner. Compared to crude FA, the efficiency of acid-treated FA is very high (99% *p*-nitrophenol was removed in the presence of 10 g L^{-1} treated FA).

Flores *et al.*[116] prepared five types of FA catalysts with immobilized ferric ions for the abatement of reactive black 5 from aqueous solution. The authors prepared the heterogeneous Fenton catalysts by incipient impregnation and ion exchange in acidic or alkaline media in the presence and absence of ultrasound. Complete decolourisation and 80% COD removal in wastewater containing the dye were observed by the authors. The efficiency of the catalyst prepared by ion exchange in alkaline media and in the presence of ultrasound energy was very poor compared to those of other heterogeneous Fenton catalysts. The catalysts prepared by incipient impregnation and iron exchange in acidic media, both in the presence and absence of ultrasound energy, displayed similar efficiency. However, the catalyst prepared by ion exchange in alkaline media and in the absence of ultrasound, exhibited higher efficiency compared to the other catalysts. The authors also observed that the catalyst prepared *via* mechanical stirring displays higher efficiency than that prepared *via* a sonication process.

Others. The efficiency of electric arc furnace dust as a Fenton catalyst for the degradation of wastewater containing pentachlorophenol (PCP) was studied by Mecozzi *et al.*[117] The authors compared the efficiency of waste materials with that of hematite and observed higher mineralization efficiency for electric arc furnace dust. TOC removals of 49.2% at a H_2O_2 : PCP ratio of 10 : 1 and a Fe : H_2O_2 ratio of 1 : 5 for unstabilized H_2O_2 and 48% at a H_2O_2 : PCP ratio of 10 : 1 and a Fe : H_2O_2 ratio of 1 : 1 for stabilized H_2O_2, respectively, were observed by the authors in the presence of electric arc furnace dust as a Fenton catalyst. In the case of hematite, the maximum TOC removal of 45.2% was achieved at a H_2O_2 : PCP ratio of 10 : 1 and a Fe : H_2O_2 ratio of 1 : 2. Blast furnace dust is also an efficient photo Fenton catalyst for the degradation of dyes in water.[118] This catalyst contains hematite, magnetite and maghemite as iron sources. The authors compared the efficiencies of both homogeneous and heterogeneous Fenton processes and found similar efficiencies. However, the rate of dye removal was very high (more than five times higher) for Fenton reactions in the presence of blast furnace dust. Similarly, iron dust also displayed higher catalytic activity for the treatment of real textile wastewater.[119]

Roasted pyrite ash or pyrite ash is a hematite-rich waste left as a residue after the production of sulphuric acid.[120] Becelic-Tomin *et al.*[121] used this waste material for the abatement of reactive blue 4 and found 99.9% decolourization and 74.3% mineralization of the dye within 30 min reaction time at a catalyst concentration of 0.2 g L^{-1}, a hydrogen peroxide concentration of 5 mM, pH 3 and an initial dye concentration of 100 mg L^{-1}.

The catalytic activities of three low-cost materials (sepiolite, red volcanic rock and iron shavings) for the treatment of simulated and actual olive mill wastewaters were compared by Martins *et al.*,[122] who found iron shavings to be the most active catalyst. At a catalyst concentration of 40 g L^{-1}, a hydrogen peroxide concentration of 35 mM and pH 3, 94% of total phenolic content, 54% of COD and 60% of TOC were removed effectively from wastewater.

Degradation of methyl orange in the presence of steel industry waste was studied by Ali *et al.*,[123] who observed 98% decolourization of wastewater containing 20 mg L^{-1} dye within

30 min at pH 2, 200 mg L^{-1} catalyst and 34 mM H_2O_2 concentrations.

Nidheesh and Gandhimathi[124] reused sludge produced in a peroxicoagulation process as a heterogeneous EF catalyst for removal of color, COD and TOC from textile wastewater. The authors observed 97% color, 47% COD and 33% TOC removal after 60 min of electrolysis. The efficiency of sludge is comparable with that of a homogeneous EF process using ferric ions as catalyst.

Iron and iron oxide-loaded materials

Iron- and iron oxide-loaded materials have been proved to be efficient Fenton catalysts for the abatement of various organic pollutants. Various materials such as activated carbon, biosorbents, clay, alumina, silica, *etc.* have been used as efficient supports for iron and iron oxides. Use of these supports enhances the efficiency of a heterogeneous Fenton process. The catalytic activity of ZVI supported on NaY zeolite is the same as that of unsupported ZVI and the conventional Fenton process.[125] The degradation efficiency for orange II of a $ZnFe_2O_4$–C_3N_4 hybrid with mass ratio 2 : 3 is 2.4 times higher than that of a simple mixture of g-C_3N_4 and $ZnFe_2O_4$.[126] One reason behind this is additional removal of pollutants by sorption of pollutants on the active pores of supports. Loading of iron on the supports did not affect their structure. For example, an insignificant change in the mesoporous structure of SBA-15 after iron loading was observed by Shukla *et al.*[127] The porous nature of supports is responsible for the effective sorption of contaminants. Yao *et al.*[128] observed that adsorption enhanced the removal of orange II under visible irradiation. Some supports also act as catalysts for the production of hydroxyl radicals. For example, C_3N_4 used as a support for $ZnFe_2O_4$ acts as a *p*-conjugated material for the formation of a heterojunction with $ZnFe_2O_4$ and as an effective catalyst for the decomposition of H_2O_2 to form $^{\bullet}OH$ radicals.[126]

Activated carbon. Activated carbon (AC) is a highly porous carbonaceous material with a large surface area. Generally, the surface area of AC is higher than 500 $m^2\ g^{-1}$, due to its high degree of microporosity.[129] Activated carbon can be produced *via* physical activation (carbonization followed by activation/oxidation) or chemical activation (impregnation followed by carbonization and activation).[129] Due to the higher surface area, large pore volume and various surface chemical functional groups in AC, it is widely used in gas purification, decaffeination, gold purification, metal extraction, water purification, medicine, sewage treatment, air filters in gas masks and respirators, filters in compressed air, *etc.*[129] AC possesses a special capacity to optimize its performance for specific applications by tailoring its physical and/or chemical properties.[130] Due to this ability, AC is used as a very efficient adsorbent for removing pollutants from water and air.

Studies also revealed that AC is a good support for iron species and can be used as a heterogeneous Fenton catalyst. Sekaran *et al.*[131] prepared mesoporous AC particles from rice husks *via* carbonization and phosphoric acid activation methods and used them for Fenton oxidation of highly non-biodegradable salt-laden wastewater from the leather industry. The prepared materials have higher surface area ranging from 345 to 439 $m^2\ g^{-1}$ and an average pore diameter ranging from 35.28 to 39.36 Å. The authors observed enhanced efficiency with the addition of AC in a Fenton process, even with low amounts of Fenton reagent. At optimum dosages of hydrogen peroxide (7.5 mmol L^{-1}), ferrous sulphate (0.3 mmol L^{-1}) and AC (10 g L^{-1}), 74% of BOD, 69% of COD, 61% of TOC and 80% of dissolved proteins were removed. The absence of sludge production during the process with the addition of AC indicates the importance of this heterogeneous catalyst in the Fenton process. Karthikeyan *et al.*[132] used the same material for the abatement of tannery wastewater. The authors reported increased biodegradability of tannery wastewater after Fenton oxidation. Also, the activation energy required for the Fenton process decreases with the addition of AC. The activation energy required for homogeneous Fenton and heterogeneous Fenton processes in the presence of AC were observed to be 44.79 and 25.89 kJ mol^{-1}, respectively. The authors also observed positive changes in enthalpy values, indicating that the Fenton process is an endothermic reaction. Also, the heterogeneous Fenton process using AC exhibits significant efficiency for the removal of dissolved protein, TOC, COD and BOD.[133] In the optimal conditions, 86% of COD, 91% of BOD, 83% of TOC and 90% of dissolved protein were removed effectively from tannery wastewater.

Karthikeyan *et al.*[134] used nanoporous AC doped with iron oxide as a heterogeneous Fenton catalyst for the abatement of *ortho*-phenylenediamine from aqueous solution. Nanoporous AC was prepared from rice husks using phosphoric acid and soaked in hydrofluoric acid. The surface areas of AC and AC doped with iron oxide were observed to be 153 $m^2\ g^{-1}$ and 38–136 $m^2\ g^{-1}$, respectively. The authors reused the material for five cycles and observed retention in the activity of the prepared heterogeneous Fenton catalyst. The amount of iron leached from the catalyst was only 0.3–0.4 mg, even after the end of 5 cycles. This indicated the higher stability of AC doped with iron oxide. From this leaching study, the authors proposed a pollutant oxidation mechanism in the presence of AC doped with iron oxide. Also, the authors observed 96% COD removal *via* heterogeneous Fenton oxidation.

Yao *et al.*[135] utilized AC fibers loaded with ferric ions as a heterogeneous Fenton catalyst for the degradation of dyes. The authors reported that the dye, namely reactive red M-3BE, was effectively degraded in the presence of AC fibers loaded with iron. The authors observed higher stability and higher activity even at neutral and basic pH values and unnecessary production of hydroperoxyl radicals during the heterogeneous Fenton reaction.

Studies also revealed that AC loaded with magnetic material is an efficient heterogeneous Fenton catalyst. Nguyen *et al.*[136] prepared magnetically loaded AC for the removal of methyl orange dye from aqueous solution. The AC had a surface area of 919.5 $m^2\ g^{-1}$. However, magnetically loaded AC had a higher surface area and porosity than those of the parent material. The authors compared the Fenton oxidation activity of AC loaded with Fe_2MnO_4 with that of AC loaded with Fe_3O_4 and found that

the first catalyst exhibited higher efficiency. After 120 min of reaction, 100% dye degradation and 59% mineralization were observed for AC loaded with Fe_2MnO_4. AC loaded with magnetite, which was prepared by a wet impregnation method and low-temperature heating in an inert atmosphere was used as a heterogeneous photo Fenton catalyst for the degradation of methylene blue from aqueous solution.[137] The AC had surface areas of 866 $m^2\ g^{-1}$ and 1000 $m^2\ g^{-1}$. The authors found complete removal of the dye after 25 min radiation in the presence of AC loaded with magnetite. Yang *et al.*[138] synthesized AC loaded with NdFeB for the removal of methyl orange and observed 97.8% dye removal after 60 min.

Zhang *et al.*[139] used AC loaded with zero-valent iron as a heterogeneous catalyst in an electro Fenton process for the removal of methyl orange from aqueous solution. More than 80% color removal after 10 min of electrolysis and more than 40% mineralization after 120 min of electrolysis were observed by the authors.

The surface chemistry of AC also affects the efficiency of heterogeneous Fenton systems. Messele *et al.*[140] studied this effect using ACs with different amounts of surface oxygenated groups. The authors used these materials as supports for zero-valent iron and used them for removing phenol from aqueous solution. The catalytic activity of zero-valent iron was not favorable in the presence of acidic oxygenated surface groups. However, heating of AC increased the efficiency of the process. This is mainly due to increased interaction between the π-electron system of AC and the phenol aromatic ring in the absence of surface oxygen content.

Tu *et al.*[141] prepared carbon derived from sewage sludge and used it as an effective support for iron oxide. The authors studied its ability to degrade acid orange II under visible irradiation and found that the catalyst pyrolyzed at 800 °C for 2 h exhibited the highest photo Fenton activity. In the optimal conditions, complete degradation and 60% mineralization of a 100 mg L^{-1} dye solution were achieved after 30 min adsorption and 60 min oxidation under visible-light irradiation. Yuan and Dai[142] synthesized mesoporous material derived from sewage sludge and loaded with α-Fe_2O_3 for the photo Fenton degradation of rhodamine B and *p*-nitrophenol. The initial contaminant degraded rapidly in the presence of UV light and the latter pollutant degraded under both UV and visible irradiation conditions.

Cleveland *et al.*[143] synthesized carbon nanotube-supported Fe_3O_4 and used it for the oxidation of bisphenol A. The authors found 97% pollutant removal in 6 h of oxidation time and the intermediates and by-products that are formed by the oxidation of bisphenol A are biologically non-toxic.

Alumina. Alumina has been used as a catalyst and supporting material for various catalytic processes. In addition to having a wide range of surface areas, alumina particles are strongly alkaline and possess ion exchange capacities, due to the presence of Al^{3+} in their framework.[144] Alumina has been used as a good supporting material for iron and its oxides for the effective degradation of various persistent organic pollutants. Degradation of 2,4-dinitrophenol by alumina-supported ferric iron was studied by Ghosh *et al.*[145] and the efficiency of a heterogeneous catalyst was compared with that of a homogeneous Fenton process using ferric iron as catalyst. The authors observed that alumina-supported ferric iron exhibits higher degradation efficiency for 2,4-dinitrophenol than that of ferric iron alone. In the optimal conditions, 92.5% and 98% of pollutants were removed by homogeneous and heterogeneous processes, respectively. Bautista *et al.*[146] prepared a highly stable Fe/γ-Al_2O_3 catalyst by an incipient wetness impregnation method and used it for the Fenton oxidation of phenol in an aqueous medium. Complete removal of phenol and almost 80% mineralization were observed by the authors at a temperature of 50 °C, initial pH 3, 100 mg L^{-1} phenol, H_2O_2 corresponding to the stoichiometric amount and 1250 mg L^{-1} catalyst. An increase in the phenol concentration to 1500 mg L^{-1} did not affect the phenol removal efficiency of the heterogeneous Fenton catalyst. However, this increase in phenol concentration reduced the mineralization efficiency of the catalyst. Iron leaching also increased at a higher phenol concentration and was mainly due to the increased amount of oxalic acid produced by the degradation of phenol. Li *et al.*[147] synthesized alumina-supported hematite and used it for the degradation of orange II in an aerated aqueous suspension under light irradiation at wavelengths longer than 320 nm. The catalytic activity of alumina-supported hematite was much higher than that of hematite. The authors also compared the efficiency of alumina-supported hematite with that of silica-supported hematite and found higher efficiency and stability with alumina-supported hematite. Alumina-supported Fe_2O_3 also displayed higher activity for polyacrylamide degradation.[148] The authors also noticed a significant effect of the preparation conditions, such as the impregnated material and trace elements, on the catalytic activity. A Fe^{3+} catalyst prepared with $Fe(NO_3)_3$ as impregnated material exhibited better catalytic activity than that using $FeSO_4$. The addition of trace elements to Fe_2O_3/Al_2O_3 also enhanced its efficiency. Among trace elements (Cu, Mo, Zn, Co and Mn), Cu displayed higher catalytic activity. Sono Fenton degradation of C.I. acid orange 7 using a Fe_2O_3/Al_2O_3 catalyst was studied by Zhong *et al.*[149] Ultrasonic irradiation causes a reduction in the aggregate size of the spent catalyst after dispersion in water. This catalyst also displayed higher efficiency in the optimal conditions.

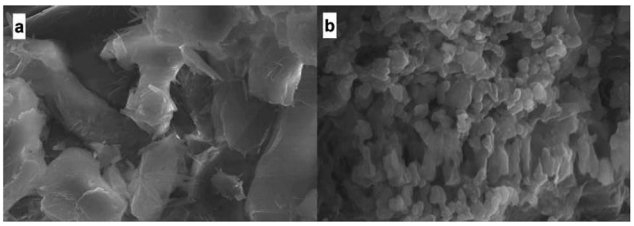

Fig. 4 SEM images of (a) MSP and (b) Fe-MSP. Figure taken from ref. 150.

Biosorbents. Biosorbents are used as effective supporting materials for iron species and are also used for the treatment of wastewater containing organic pollutants. The higher amount of porosity in biosorbents is responsible for the immobilization

of iron species and these iron species can act as efficient Fenton catalysts. Laiju *et al.*[150] prepared mangosteen shell powder loaded with iron (Fe-MSP) for the Fenton oxidation of stabilized landfill leachate. The amount of Fe species adsorbed on Fe-MSP was found to be 745 mg g^{-1}. Scanning electron microscopy (SEM) images of mangosteen shell powder (MSP) and Fe-MSP are shown in Fig. 4. Initially, MSP has a large amount of voids in it. After iron is loaded, the amount of voids in MSP is reduced significantly. This reduction is mainly due to effective occupancy by iron species in the biosorbent. More than 80% COD removal from stabilized landfill leachate was observed by the authors in the optimal operating conditions of pH 3, catalyst concentration of 1750 mg L^{-1} and hydrogen peroxide concentration of 0.26 M. The authors also compared the efficiency of a heterogeneous Fenton process in the optimal conditions with that of a homogeneous Fenton process using ferrous sulphate as catalyst. By comparing the density, the amount of iron in 1750 mg L^{-1} Fe-MSP was found to be 875 mg L^{-1} and the same amount of ferrous ion was utilized for the homogeneous Fenton process. The heterogeneous Fenton process using Fe-MSP was found to be more effective than the homogeneous Fenton process. The COD removal efficiencies of the homogeneous and heterogeneous Fenton processes were observed to be 70% and 81%, respectively, after 60 min.

Daud and Hameed[151] prepared rice husk ash-supported ferric oxide by an incipient impregnation method and used it for the decolourization of acid red 1 in aqueous solution. The surface area, pore size and pore volume of the catalyst were 61.33 m^2 g^{-1}, 135.52 Å and 0.21 cm^3 g^{-1}, respectively. After 120 min, 96% of acid red 1 was decolorized effectively in the optimal operating conditions. Iron impregnated in rice husk ash also displayed higher efficiency for the degradation of reactive black 5.[152] Tekin *et al.*[153] prepared activated walnut shells doped with Fe^{3+} and used them for oxidation of benzoic acid. The authors concluded that the catalyst prepared was not very active in the treatment of benzoic acid because the degradation efficiency achieved was very low.

Fiber. Various fiber materials have been used as effective supporting materials in Fenton processes. Among these materials, polyacrylonitrile (PAN) fiber has received much attention. Wu *et al.*[154] used amidoxime-modified PAN fiber with $FeCl_3$ for the degradation of rhodamine B and observed an increase in the iron concentration in the fiber with increase in the iron ion concentration in solution, reaction temperature and reaction time. The authors also observed complete decolourization of a pollutant in the optimal conditions. Chi *et al.*[155] prepared a modified PAN fiber by reacting 27.9 g PAN mesh with a 1 L solution of 49.6 g L^{-1} hydroxylamine sulphate and 23.17 g L^{-1} dihydrazine sulphate at pH 9.5, 100 ± 2 °C under reflux for 2 h with constant stirring. The authors used this heterogeneous Fenton catalyst for the removal of endocrine-disrupting compounds (EDCs) and pharmaceutical and personal care products (PPCPs) from municipal wastewater in a continuous stirred tank reactor. More than 90% of EDCs, 40% of PPCPs, 100% of BOD, 82% of estrogenic potency and 68% of turbidity were removed effectively from wastewater in the optimal conditions and 30–40% mineralisation was achieved. A modified PAN catalyst is effective for the degradation of maleic acid in aqueous solution.[156,157] In the optimal conditions, 95% maleic acid removal and 65% mineralization were observed by the authors.[156] Zhao *et al.*[158] prepared a modified PAN nanofiber–Fe complex *via* the amidoximation and subsequent Fe coordination of a PAN nanofiber using an electrospinning technique. The authors observed that the prepared catalyst was very effective for the photo Fenton degradation of three types of textile dyes, namely reactive red 195, reactive blue 4 and acid blue 7.

Polytetrafluoroethylene (PTFE) fiber is also used as a supporting material. Ding *et al.*[159] prepared modified PTFE fibers by graft polymerization of acrylic acid to introduce carboxyl groups onto the fiber surface, which are used to coordinate with transition metal ions (Fe^{3+} and Cu^{2+}) or rare-earth metal ions (Ce^{3+}). A significant increase in the metal content, especially the Fe^{3+} and Cu^{2+} content, of the catalysts was achieved with an increase in metal ion concentrations in solution, a higher coordination temperature and a higher grafting degree of the PTFE fiber. Fe^{3+} ions fixed on the fiber exhibited more powerful catalytic performance than fixed Cu^{2+} and Ce^{3+} ions. Because of a synergistic effect between Fe^{3+} and Cu^{2+} ions, modified Cu–Fe bimetallic PTFE fiber complexes displayed higher dye degradation efficiency. This efficiency depends more on the Cu/Fe molar ratio, which was found to be optimal at 2.87. Li *et al.*[160] used grated Cu–Fe bimetallic PTFE fiber complexes with a Cu/Fe molar ratio of 2.87 for the degradation of reactive red 195, reactive yellow 145, and reactive blue 222 under UV irradiation. Complete decolourization and a higher amount of mineralization were observed in the optimal operating conditions.

Li *et al.*[161] used three carboxylic fibers including alginate fibers and polyacrylic acid-grafted polypropylene (PP) and PTFE fibers to prepare different Fe^{3+}–carboxylic fiber complexes and found that alginate fiber could react more easily with Fe^{3+} ions than grafted PP or PTFE fibers to form complexes. The efficiency of these complexes for degradation of reactive red 195 was evaluated. In the dark or under light irradiation, all three complexes display the ability to degrade this dye in an aqueous medium. Among these fiber complexes, the Fe^{3+}–alginate fiber complex exhibited higher catalytic activity. Activated carbon fibers are also a good support medium for iron species. Wang *et al.*[162] synthesized an Fe-activated carbon fiber complex and used it for dye degradation. The authors concluded that the higher adsorption capacity of the support enhances the Fenton catalytic performance of the fiber complex.

Silica. Mesoporous silica has also been widely used for supporting iron and its oxides. Among all silica materials, SBA-15 and MCM-41 have received great attention from various researchers. Zhong *et al.*[163] synthesized iron-doped SBA-15 (Fe_2O_3/SBA-15) and used it as a heterogeneous catalyst for the degradation of C.I. acid orange 7 using a sono-photo Fenton process. Significant dye removal was observed in the presence of the prepared catalyst and its efficiency increased with increases in hydrogen peroxide concentration, ultrasonic power, and Fe_2O_3/SBA-15 loading, but decreased with increases in initial pH and initial dye concentration. Wang *et al.*[164] synthesized FeO_x-loaded SBA-15 by a simple physical vapor infiltration

method using ferrocene as iron source and used it for the degradation of acid orange 7 in aqueous solution. FeO_x contains a larger amount of ferrous ions due to its low degree of crystallization and large amount of defects and has a larger surface area and more active sites than iron oxide crystals.[164,165] Its large amount of ferrous ions and large surface area make FeO_x–SBA-15 an efficient Fenton catalyst. Almost complete removal of dye within 10 min of reaction was observed by the authors at pH 3, $[H_2O_2] = 15$ mM, and $[FeO_x/SBA\text{-}15] = 0.6$ g L^{-1}. Shukla *et al.*[127] synthesized Fe-loaded mesoporous SBA-15 for the degradation of 2,4-dichlorophenol in aqueous solution and observed complete removal of pollutant after 4 h with the addition of 0.1 g catalyst.

The large surface area of MCM-41 helps this material to be a good support in Fenton processes. The surface area of MCM-41 was found to be 1400 m^2 g^{-1}.[166] Nogueira *et al.*[166] used magnetite-loaded MCM-41 for the abatement of methylene blue and observed complete removal of dye and an average mineralization of 43% within a reaction time of 180 min. The authors also compared the dye removal efficiency of magnetite-loaded MCM-41 with those of MCM-41 and magnetite and found that the efficiencies of these catalysts follow this order: magnetite-loaded MCM-41 > MCM-41 > magnetite. Pradhan and Parida[167] synthesized Al_2O_3–MCM-41 with a large surface area and a Si/Al ratio of 10 and iron was loaded in the composite material. The synthesized material had a large BET surface area (207–1244 m^2 g^{-1}), narrow pore size (2.4–2.7 nm) and high pore volume (0.370–2.37 cm^3 g^{-1}). The authors used this material for the degradation of methylene blue and observed that a catalyst prepared with 5% wt of iron displays higher Fenton catalytic activity. Complete removal of the pollutant within 5 min of reaction was observed by the authors in the optimal conditions.

Due to its unique properties and structure, silica gel, which is a highly microporous material, is also used as a support for catalysts. Zhao *et al.*[168] used silica gel for supporting ferrous ions and evaluated its degradation efficiency under visible irradiation. Sulforhodamine B and 2,4-dichlorophenol were utilized as model pollutants. The degradation of sulforhodamine B in water and its mineralization reached 100% and 72.3%, respectively, after 180 min. At the same time, 80% of 2,4-dichlorophenol was removed effectively after 150 min of irradiation. Chen *et al.*[169] loaded cationic cyclopentadienyl iron complexes of an arene on silica gel and used this as an effective photo Fenton catalyst for the degradation of dyes under visible light. Rhodamine B and crystal violet were utilized as model dyes and almost complete removal of both dyes was achieved in the optimal operating conditions.

Miao *et al.*[170] used hierarchically porous silica for the support of Fe_2O_3 and used it as a photo Fenton catalyst for the degradation of the azo dye orange II. The chemical and physical characteristics of different porous materials were combined in a hierarchically porous material, which resulted in enhanced molecular diffusion and mass transfer by the novel structure. The authors synthesized this catalyst by sol–gel and wetness impregnation methods and found it to be an effective catalyst for dye degradation. More than 90% of the dye was degraded under visible-light irradiation. Even though the iron content in the prepared catalyst was less than 40% pure Fe_2O_3, the catalytic activity of Fe_2O_3 supported on hierarchically porous silica is much higher than that of pure Fe_2O_3.

Gan and Li[171] extracted sodium silicate from rice hulls *via* a modified alkali extraction method and prepared a rice hull-based silica-supported iron catalyst for the degradation of rhodamine B. An enhancement in dye degradation was observed with the addition of NaCl and Na_2SO_4 to the system. A stepwise addition strategy also enhanced the degree of mineralization. Almost complete removal of the dye was observed within 10 min of reaction time.

Zeolites. Zeolites are the aluminosilicate members of the microporous solids family and act as "molecular sieves", which can accommodate a wide variety of cations such as Na^+, K^+, Ca^{2+}, Mg^{2+}, *etc.*[172] Analcime, chabazite, clinoptilolite, heulandites, natrolite, phillipsite and stilbite are examples of common mineral zeolites.[172] Based on the dimensions of their micropores, zeolites are classified as small, medium and large pore size, where the channels are constituted by eight, ten and twelve oxygen atoms, respectively.[173] Due to their highly porous nature, zeolites are used extensively as supports for various catalysts. Use of Fe-zeolites has the following advantages over the homogeneous Fenton process:[174] (a) They are active even at nearly neutral pH, (b) pollutant degradation occurs due to the combination of adsorption and oxidation and (c) they can easily be recycled, as their particle size is in the μm range. Fukuchi *et al.*[175] evaluated the 2,4,6-tribromophenol degradation efficiency of iron-loaded natural zeolite and observed insignificant removal of the pollutant. However, the addition of a reducing agent such as ascorbic acid or hydroxylamine enhanced the efficiency of the heterogeneous Fenton process. Gonzalez-Olmos *et al.*[174] used Fe-ZSM5 and Fe-Beta for the degradation of phenol, imidacloprid and dichloroacetic acid. The authors found that Fe-ZSM5 produces reactive species at a higher rate than Fe-Beta. The complex tris(1,10)-phenanthroline-iron(II) loaded on the NaY type of zeolite is also an efficient photo Fenton catalyst for the degradation of dyes in aqueous solution.[176] Yan *et al.*[177] loaded various amounts of iron on a ZSM-5 zeolite membrane with a Si/Al ratio of 80 and used it for the treatment of wastewater containing phenol. Uniform dispersion of Fe_2O_3 on the surface of the ZSM-5 zeolite membrane support was observed by the authors. The efficiency of the prepared catalyst was evaluated in a membrane reactor and the highest activity (about 95% phenol degradation and 45% TOC removal) was achieved after the test ran continuously for 7 h. By the integration of membrane separation with a heterogeneous Fenton process using a FeY catalyst, Zhang *et al.*[178] observed higher dye removal efficiency. Almost 97% acid orange II degradation was achieved in a membrane–heterogeneous Fenton process at a catalyst dosage of 1 g L^{-1} and a residence time of 120 min.

Others. Polyacrylamide hydrogels loaded with iron also exhibited higher catalytic activity for dye degradation.[179] Authors used this catalyst for the electro Fenton treatment of two dyes, reactive black 5 and blue Sella solid. The prepared catalyst with a ferrous-to-ferric molar ratio of 1 : 2 displays the maximum dye removal efficiency. Almost complete removal of

dye was observed in the optimal conditions. Furthermore, authors used this catalyst for the treatment of simulated effluent which was polluted by a real dye used by the leather dyeing industry and observed 90% decolorization efficiency after 2 h of electrolysis.

González-Bahamón *et al.*[180] synthesized iron-loaded commercial polyethylene *via* three different methods: (1) acid pretreatment of polyethylene followed by impregnation in $Fe(NO_3)_3$ solution, (2) photocatalytic pretreatment of polyethylene in the presence of TiO_2 followed by the forced hydrolysis of $Fe(NO_3)_3$, and (3) a direct photo Fenton reaction accompanied by deposition of iron on the surface of polyethylene. Among these methods, the photo Fenton functionalization/Fe deposition method generated a highly efficient catalyst. Total degradation of resorcinol and 50% mineralization were observed after 40 and 60 min of photo Fenton oxidation, respectively.

Using a hydrothermal method, Vu *et al.*[181] carried out partial isomorphous substitution of Cr by Fe in the framework of MIL-101 and used this material as a photo Fenton catalyst for the removal of the dye reactive red 195. After the synthesis process, almost 25% of the Cr atoms in the MIL-101 framework were substituted by Fe atoms. Almost complete removal of the pollutant was observed after 90 min of irradiation.

Soil

Laterite. Due to intensive weathering that occurs under tropical and subtropical climatic conditions, accumulation of hydrated iron and aluminium oxides occurs in the soil, which results in the formation of laterite.[182] Laterite is a porous soil which is coarse in texture and rich in minerals such as iron, aluminum, manganese and titanium but poor in nitrogen, phosphoric acid, potash and lime.[183] XRD analysis of laterite samples indicates that goethite and hematite are the main iron constituents in laterite.[184] The specific surface area of laterite is in the range of 23.12 $m^2\ g^{-1}$ and its pore volume is in the range of 0.066 $cm^3\ g^{-1}$.[184] Due to the high concentration of iron in laterite soil, it can be used as a heterogeneous Fenton catalyst for the abatement of various persistent organic pollutants. Manu and Mahamood[183] studied the degradation of paracetamol by a photo Fenton process in the presence of a laterite catalyst. Complete removal of the pollutant and 77% mineralization were observed by the authors after 120 min of heterogeneous photo Fenton oxidation. Karale *et al.*[185] observed complete degradation of 2-aminopyridine by a heterogeneous photo Fenton process and 90% degradation by a heterogeneous Fenton process using laterite as a catalyst. The authors also observed that the optimal laterite concentration was much lower compared to the hydrogen peroxide concentration. For the Fenton process, the ratio of the optimum value of hydrogen peroxide concentration to that of laterite concentration was 40–65 : 1. Khataee and Pakdehi[184] used laterite soil as a heterogeneous Fenton catalyst for the removal of sodium azide and reported that 97% of pollutant was removed effectively from aqueous solution after 60 min of oxidation.

Clay. Clay is a fine-grained soil that contains one or more clay minerals and has a layered structure composed of silicate sheets bonded to aluminium oxide/hydroxide sheets.[186] Clay minerals are composed mainly of hydrous aluminium phyllosilicates with variable amounts of iron, magnesium, alkali metals, alkaline earth metals and other cations.[187] As clays are natural, abundant, inexpensive, and environmentally friendly, the use of clays as heterogeneous Fenton catalysts is a promising alternative for decontamination of soils, groundwater, sediments, and industrial effluents.[188] Djeffal *et al.*[189] used iron-rich red clay as a heterogeneous Fenton catalyst for the degradation of phenol in an aqueous medium and observed compete removal of the pollutant and 70% mineralization of the solution after 6 h of contact time.

However, one problem related to the use of clay as a Fenton catalyst is its low iron concentration. Even though clay contains larger amounts of exchangeable cations, it is very difficult to increase the iron concentration in clay minerals by cation exchange methods.[190] This difficulty can be rectified by pillaring and impregnation methods.

Pillaring is the process by which a layered compound is transformed into a thermally stable micro- and/or mesoporous material with retention of its layer structure.[191] Pillared clays are a class of microporous solid acids derived *via* the intercalation of polycations into the galleries of layered silicates with mica-like or 2 : 1 sheet structures.[192] A pillaring agent is any compound which can be intercalated between adjacent layers of a layered compound, maintaining the spacing between adjacent layers upon removal of the solvent and producing an experimentally observable pore structure between the layers.[191] The most commonly used pillaring agent for the synthesis of pillared clay is the Keggin-like ion $[Al_{13}O_4(OH)_{24}(H_2O)_{12}]^{7+}$, which is particularly introduced between layers of smectite clays such as montmorillonite, beidellite or saponite.[190] The pillaring process consists of three steps.[193] Polymerization of a multivalent cation and intercalation of the polycation into the interlayer space of clay are the first two steps in this process. The final step is thermal treatment of the intercalated clay mineral or a calcination process, which dehydrate and dehydroxylate the pillaring agent to form a fixed metal oxide pillar with high thermal stability and a large surface area.[194] The fixed, rigid metal oxide formed after the calcination process is known as a pillar, and the pillars prop up the clay layers and prevent their collapse.[195] Iron can be introduced into pillared clays by adding iron salts to the pillaring solution and a subsequent calcination process.[192] De León *et al.*[196] synthesized iron pillared clay for the abatement of methylene blue and observed more than 87% dye removal. The authors also observed little leaching of iron species from the iron pillared clay. Even after 350 h of activity in a continuous flow reactor, Tatibouët *et al.*[197] observed less than 2% iron leaching. This is an additional advantage of iron pillared clay.

Impregnation is the other method of introducing iron into clay. There are two types of impregnation methods:[192] wet impregnation and incipient wetness impregnation. In the first method, clay is added to a solution of an iron salt and heated for some time to evaporate water. Calcination of the dried product is required for better catalytic activity. The second method is similar to the first method. However, in the second method, the

volume of the iron salt solution is equal to the total pore volume of the clay particle. Hassan and Hameed[186,188] prepared iron-containing ball clay for the oxidative removal of reactive blue 4 and acid red 1 from aqueous solution. After 180 min of reaction, 99% of acid red 1 was degraded in the presence of iron-containing ball clay. Moreover, the same amount of reactive blue 4 was degraded within 140 min of reaction.

Bentonite. Bentonite is a well-known adsorbent clay, usually formed *via* weathering of volcanic ash in the presence of water.[198] Based on its dominant cationic element, bentonite is classified as sodium bentonite, potassium bentonite, calcium bentonite and aluminium bentonite. Pillared bentonite is a well-known heterogeneous Fenton catalyst. Arora *et al.*[199] used bentonite pillared by hydroxyl iron as a photo Fenton catalyst for the degradation of rose bengal and observed optimal removal efficiency at neutral pH. Catrinescu *et al.*[200] prepared Romanian bentonite pillared by Al and Al–Fe and used it for the oxidative removal of phenol from aqueous solution. The authors observed higher activity for both catalysts, even though clay pillared by Al–Fe was more stable than clay pillared by Al. Bentonite pillared by Al–Fe also displayed higher oxidative removal efficiency for the azo dye X-3B under solar light irradiation.[201] Photo Fenton catalytic removal of tetracycline using bentonite pillared by Fe–Ce was studied by Zhang *et al.*[202] who observed 98.13% pollutant degradation under conditions of 15 mmol L^{-1} H_2O_2, 0.5 g L^{-1} catalyst dosage, initial pH 3, 11 W UV lamp power and 60 min reaction time. A Fe-bentonite clay nanocomposite film also exhibited higher pollutant removal efficiency. Feng *et al.*[203] used this catalyst for the abatement of orange II from an aqueous medium and observed 100% discoloration and 50–60% TOC removal within 120 min of UV irradiation.

Laponite. laponite is a synthetic clay mineral with various industrial applications. laponite is a unique speciality additive: a layered silicate manufactured from naturally occurring inorganic mineral sources.[204] The time-dependent microstructure evolution and physical properties of laponite have received much attention.[205,206] The Fenton activity of laponite has also received much attention in recent years. Feng *et al.*[207] used a laponite clay-based Fe nanocomposite for the photo Fenton degradation of orange II and observed 70% mineralization of the dye within 90 min of UV irradiation. With the help of XRD analysis, the authors found that the heterogeneous catalyst mainly contained Fe_2O_3 (maghemite) and $Fe_2Si_4O_{10}(OH)_2$ (iron silicate hydroxide).[207,208] The pore volume and surface area of the catalyst were also very high. The specific surface area and total pore volume of the laponite clay-based Fe nanocomposite were found to be 472 m^2 g^{-1} and 0.547 cm^3 g^{-1}, respectively.[208] Complete decolourization of reactive red HE-3B within 30 min and 76% TOC removal within 120 min were observed by the authors in the presence of a laponite–Fe composite catalyst.[208] Sum *et al.*[209] used the same catalyst for the abatement of the azo dye acid black 1 and observed complete discoloration and over 90% TOC removal after 90 min reaction. Thermal treatment during the synthesis of the catalyst also affects its efficiency. Iurascu *et al.*[210] used Fe-treated laponite prepared by intercalation and pillaring of laponite clay with an iron salt for the degradation of phenol in aqueous solution. After intercalation, a calcination process was carried out at four different temperatures (250, 350, 450, and 550 °C). The authors also synthesized the catalyst in the absence of thermal treatment. Finally, the authors found that the catalyst prepared with thermal treatment and calcined at 350 °C exhibits higher Fenton activity than the other catalysts. Complete conversion of phenol after 5 min of photo Fenton oxidation was also observed by the same authors.

Montmorillonite. Montmorillonite is a member of the smectite group and a very soft phyllosilicate group mineral.[211] A negatively charged layer is formed in montmorillonite *via* substitution of Al^{3+} by Mg^{2+} in its octahedral sheet and this charge is compensated by hydrated cations adsorbed in the interlamellar space.[212] These cations are easily substitutable. Therefore, both the cation exchange ability and the negative charge of montmorillonite make it suitable for embedding ionic nanoparticles *via* an exchange method.[213] This property results in the formation of efficient heterogeneous Fenton catalysts based on montmorillonite. De León *et al.*[214] used montmorillonite pillared by iron for the degradation of 2-chlorophenol in the presence of UV light. The montmorillonite clay used for the preparation of the catalysts was rich in calcium and after the pillaring process the iron content increased from 1.1% to 6.1%. Almost complete degradation of the pollutant was observed by the authors. The authors also compared the 2-chlorophenol degradation efficiency of montmorillonite pillared by iron with those of goethite and zero-valent iron. The catalytic efficiency of montmorillonite pillared by iron was comparable with that of zero-valent iron and the efficiencies of both catalysts were very much higher than that of goethite. Pillared montmorillonite-supported ferric oxalate was used as a heterogeneous photo Fenton catalyst for the degradation of amoxicillin in an aqueous medium.[212] More than 99% pollutant degradation and 84% COD removal were observed by the authors in optimal operating conditions. Zhang *et al.*[213] used a montmorillonite catalyst intercalated with trinuclear iron clusters for the photo Fenton degradation of phenol. The trinuclear iron acetato cluster contains a regular triangular Fe_3O unit with iron octahedra, which are connected by six bridging acetate groups. The montmorillonite catalyst intercalated with trinuclear iron clusters displayed higher catalytic activity compared to a traditional montmorillonite catalyst intercalated with iron hydroxide, which is mainly due to its larger surface area and more active iron species. Muthuvel *et al.*[215] synthesized a Fe-encapsulated montmorillonite catalyst for the degradation of acid yellow 17 dye and observed higher removal efficiency even at neutral pH. A montmorillonite nanocomposite pillared by mesoporous iron-modified Al_2O_3 nanoparticles was found to be an effective photo Fenton catalyst for the degradation of acid blue and reactive blue.[216] Significant roles for ammonia, cetyltrimethylammonium bromide, octylamine and the calcination temperature during the synthesis of the heterogeneous catalyst were also observed by the authors. Initially, pure montmorillonite was a micro/mesoporous material and its mesoporosity developed after pillaring with Al_2O_3 nanoparticles. Modification

of this mesoporous material with iron resulted in a highly active Fenton catalyst with the ability to degrade 500 mg L^{-1} dye within 30 min. Kouraichi *et al.*[217] synthesized a heterogeneous Fenton catalyst by intercalating and pillaring montmorillonite with Al–Fe, Al–Co, Al–Cu, Al–Fe–Cu or Al–Fe–La polyoxocationic solutions and used it for the degradation of methyl parathion. The pillaring process linked metals to Al–O in the alumina octahedral sheets and Si–O in the silica tetrahedral sheets. The authors observed higher pollutant removal in a sono Fenton process than in a Fenton process.

Saponite. Saponite is a trioctahedral mineral of the smectite group with chemical formula $Ca_{0.25}(Mg,Fe)_3((Si,Al)_4O_{10})(OH)_2 \cdot n(H_2O)$.[218] Pillared saponite was found to be an effective heterogeneous Fenton catalyst for the degradation of dyes in aqueous solution.[219] Impregnation with iron was carried out using four iron salts as precursors, namely Fe(II) acetate, Fe(II) oxalate, Fe(II) acetylacetonate and Fe(III) acetylacetonate. The iron species were dispersed over the intercalated saponite clay. The authors also observed that the type of precursor used for the preparation of the catalyst has a significant effect on its Fenton catalytic activity. The catalyst prepared using Fe(II) oxalate displayed higher dye removal efficiency than other catalysts. In optimal conditions, 99% dye degradation and 91% mineralization were observed after 4 h of the oxidation process.

Sepiolite. Sepiolite is a complex magnesium silicate clay mineral with typical formula $Mg_4Si_6O_{15}(OH)_2 \cdot 6H_2O$ and is present in various forms such as fibrous, fine particulate, and solid forms.[220] Sepiolite contains blocks and tunnels, which grow in the direction of the fibers,[221] and its basic unit cell consists of silicon–oxygen tetrahedra and magnesium–oxygen octahedra.[222] This unique fibrous structure provides a larger surface area, good thermostability and corrosion resistance properties in sepiolite clays.[222] Iglesias *et al.*[223] synthesized iron-loaded sepiolite and used it as a heterogeneous electro Fenton catalyst for the degradation of reactive black 5. The authors observed 97% dye removal in acidic conditions. Gao *et al.*[224] prepared polyhydroxyl-iron/sepiolite by a facile method and used it as an effective Fenton catalyst for the degradation of rhodamine B and 4-nitrophenol solutions in the presence of visible light. The catalyst was very efficient in a wide range of pH values. Almost complete dye degradation and more than 90% mineralization were observed by the authors in acidic conditions. At the same time, 95.5% pollutant degradation, 73.1% COD removal and 80% TOC removal were observed in 4-nitrophenol solution. Fe–Mn sepiolite was also found to be an effective catalyst for the degradation of dyes in aqueous solution.[225] α-Fe_2O_3, γ-Fe_2O_3 and MnO are the main constituents of Fe–Mn sepiolite. More than 90% decolorization from 50 mg L^{-1} reactive brilliant blue solution was observed by the authors after 60 min of reaction.

Vermiculite. Vermiculite is a hydrous phyllosilicate mineral which expands greatly with the application of heat.[226] This clay is an example of a 2 : 1 type clay; that is, vermiculite contains two tetrahedral sheets for every one octahedral sheet. In vermiculite, octahedral alumina or magnesia sheets are sandwiched between two tetrahedral silicate sheets.[227,228] Purceno *et al.*[229] mechanically ground vermiculite to expose the iron ions present in the layer structure and used it as a heterogeneous Fenton catalyst for the degradation of indigo carmine. However, an insignificant change in the iron concentration was found after the grinding process. The higher concentration of structural iron in vermiculite (70% Fe^{3+} and 30% Fe^{2+}) helps the clay particles act as an effective Fenton catalyst. The dye removal profile in the presence of vermiculite was the same as that in the homogeneous Fenton process. Vermiculite pillared by iron also displayed higher Fenton catalytic activity for dye degradation. Chen *et al.*[230] used a vermiculite catalyst pillared by iron for the degradation of reactive brilliant orange X-GN in the presence of UV irradiation. Almost complete removal of the dye and 54% mineralization of a dye solution containing 100 mg L^{-1} reactive brilliant orange X-GN within 75 min of photo Fenton oxidation were observed.

Kaolinite. Kaolinite is a layered silicate clay mineral with chemical formula $Al_2O_3 \cdot 2SiO_2 \cdot 2H_2O$ in which one tetrahedral sheet is linked through oxygen atoms to one octahedral sheet of alumina octahedra.[231,232] Kaolinite is a soft, earthy white mineral exhibiting low shrink–swell and cation exchange capacities, usually produced by chemical weathering of aluminium silicate minerals such as feldspar.[233] Kaolin or china clay is a rock enriched with kaolinite. Kaolinite and kaolin have been used as efficient supports in heterogeneous Fenton processes. Kaolinite loaded with ferric oxalate was found to be an efficient photo Fenton catalyst for the degradation of 4-nitrophenol.[234] Ayodele[235] studied phosphoric acid treatment of a kaolinite-supported ferrioxalate photo Fenton catalyst for the degradation of amoxicillin in aqueous solution and observed an increase in the specific surface area of kaolinite with acid treatment. Ferrioxalate loaded on kaolinite treated with 10 M phosphoric acid has a higher iron content, which resulted in higher pollutant degradation efficiency. Almost 99% of amoxicillin was degraded in 8 min of UV irradiation. Kaolin as a support material reduced the aggregation of nanoscale zero-valent iron and improved the adsorption of direct black G.[236] This enhanced the catalytic activity of zero-valent iron, with 87% dye degradation and 54.6% total organic carbon removal in optimal conditions. Guo *et al.*[237] synthesized kaolin loaded with Fe_2O_3 and used it for the photo Fenton degradation of rhodamine B. After loading with iron oxide, the specific area of kaolin increased from 19.47 to 39.32 m^2 g^{-1}. Also, the authors observed 98% dye degradation and 66% mineralization in 120 min.

Heterogeneous Fenton-like catalysts

Degradation of persistent organic pollutants using heterogeneous Fenton-like processes has also received significant attention in recent years. Elements such as chromium, cerium, copper, cobalt, manganese, ruthenium, *etc.* have multiple redox states and have the ability to decompose H_2O_2 into $HO^{\bullet}$ *via* conventional Fenton-like pathways as in eqn (17).[238,239] Therefore, a catalyst containing the above elements undergoes a heterogeneous Fenton-like process in the presence of hydrogen peroxide and organic pollutants. Kalal *et al.*[240] prepared a copper pyrovanadate photo Fenton catalyst by a wet chemical

method and used it for the degradation of neutral red and azure B. The authors found that the photo Fenton activity of copper pyrovanadate is much higher than that of CuO and V_2O_5. This enhanced efficiency of the prepared catalyst is mainly due to simultaneous activation of hydrogen peroxide in the presence of copper and vanadium. Angı *et al.*[241] synthesized copper oxide nanoparticles by sonication of copper acetate monohydrate and hydrogen peroxide. The heterogeneous Fenton activity of the prepared material for the degradation of methylene blue was also tested. Initially, the rate of dye removal was very high and it then decreased with reaction time. Cavitation-induced surface defects in the catalytic process are the main reasons behind this decrease in dye removal rate and loss in the catalytic activity of the prepared catalyst after annealing of products.

$$M^{(n-1)+} + H_2O_2 \rightarrow M^{n+} + HO^{\cdot} + OH^{-} \quad (17)$$

Transition metals loaded on various supports also displayed high Fenton-like catalytic activity. Ghosh *et al.*[242] used SBA-15 loaded with Cu nanoparticles for the removal of various dyes, such as 4-nitrophenol, methyl orange, congo red, rhodamine B, methylene blue and mixtures of dyes, in the presence of excess $NaBH_4$. This material exhibits higher catalytic activity for the degradation of both single and mixed dyes. Dyes were removed within 8 min of reaction time with high first-order reaction rate constants. Pradhan *et al.*[243] synthesized a mesoporous Cu/Al_2O_3–MCM-41 nanocomposite and used it as a heterogeneous photo Fenton-like catalyst for the degradation of phenol, 2-chloro-4-nitrophenol and 4-chloro-2-nitrophenol in aqueous solution. The catalyst was very efficient in the presence of sunlight, mainly due to its small particle size, easy reducibility of copper metal, stabilization of Cu^{2+} in the mesoporous support Al_2O_3–MCM-41, good textural property and higher activity in visible light. Nearly 100% degradation of all the phenolic compounds within 45 min occurred at pH 4. Copper-loaded bentonite displayed high photo Fenton activity for rhodamine B degradation.[244] Almost 68% of the dye was removed in the optimal conditions. Electro Fenton degradation of reactive black 5, imidacloprid, di-2-ethylhexyl phthalate and 4-nitrophenol using Mn-loaded alginate was studied by de Dios *et al.*[245] The authors found higher activity and stability of the synthesized catalyst in both batch and continuous-flow modes.

Leaching of catalyst and pollutant degradation mechanism

Leaching of metal from a catalyst is an important factor. Continuous leaching of metal ions results in deactivation of a heterogeneous catalyst and secondary pollution due to leached metal ions. Some catalysts exhibit very low leaching properties, while others display higher leaching characteristics. Hematite displays very low leaching properties. Araujo *et al.*[64] determined the iron content after 20 min of a reaction and 50% dye degradation during this time. In the presence of UV light, Fe ions leaching from a montmorillonite catalyst intercalated with a trinuclear iron cluster increased from 0 to 3 mg L^{-1} initially and then decreased continuously.[213] A similar trend was observed by Nidheesh *et al.*[80] for the leaching properties of magnetite. The ferrous ion concentration in the solution increased to 1.63 mg L^{-1} within 30 min during electro Fenton oxidation of rhodamine B and then decreased to less than 0.5 mg L^{-1} after 150 min of electrolysis. During this time, the ferric ion concentration increased continuously and reached a maximum after 135 min of electrolysis. Acid-activated fly ash exhibited the same properties during the degradation of *p*-nitrophenol.[115] The authors proposed that the relationship between the total iron concentration in the solution and the reaction time is:[115]

$$C = -0.002t^2 + 0.248t \quad (18)$$

The leaching of metal ions from a catalyst also depends on the solution pH. Ding *et al.*[159] observed decreased leaching

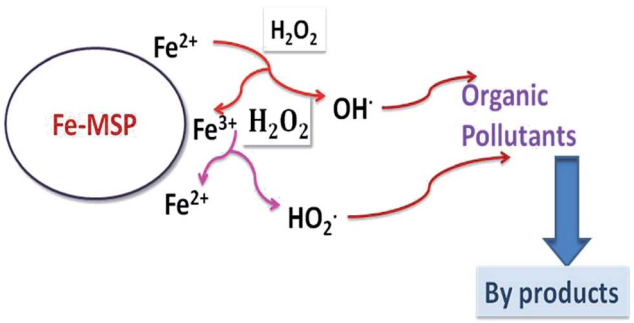

Fig. 5 Contaminant degradation mechanism of Fe-MSP. Figure taken from ref. 150.

Table 7 Metal leaching properties of various heterogeneous Fenton catalysts

No.	Catalyst	Leached metal concentration
1	Ground vermiculite[229]	Soluble Fe = 0.083 μg L^{-1}
2	Fe^{3+} loaded on Al_2O_3 (ref. 145)	Soluble Fe = 6 mg L^{-1}
3	Magnetite[80]	Fe^{3+} = 3.85 mg L^{-1} Fe^{2+} = 1.63 mg L^{-1}
4	Montmorillonite intercalated with trinuclear iron cluster[213]	Fe ion = 3 mg L^{-1}
5	Acid-activated fly ash[115]	Fe^{3+} ~6.5 mg L^{-1} Fe^{2+} ~6 mg L^{-1}
6	Mangosteen shell powder loaded with iron[150]	Fe^{3+} = 1.3 mg L^{-1} Fe^{2+} = 6 mg L^{-1}

properties with a modified polytetrafluoroethylene fiber catalyst. Leaching of iron from the heterogeneous catalyst also increased with the iron concentration. With an increase in pH from 3 to 9, ferric iron leached from the catalyst decreased from 0.49 mg L^{-1} to 0.07 mg L^{-1}. Similarly, leaching of copper and iron from Cu–Fe bimetallic polytetrafluoroethylene fiber complexes also decreased with an increase in the pH of the solution. The leaching properties of some heterogeneous Fenton catalysts are given in Table 7.

The pollutant degradation mechanism in the presence of a heterogeneous Fenton catalyst depends more on its metal leaching property. Fenton reactions can occur in two ways: on the surface of the catalyst or in solution. In the case of surface Fenton reactions, negligible amounts of metal ions are leached from the catalyst. The surface of the catalyst is predominantly characterized by ferrous and ferric ions. Hydrogen peroxide added to the solution reacts with these surface iron species and forms hydroxyl radicals. For example, mangosteen shell powder loaded with iron (Fe-MSP) follows this contaminant degradation mechanism.[150] Pollutant degradation from stabilized landfill leachate in the presence of Fe-MSP catalyst is shown in Fig. 5.

Pollutant degradation in the presence of a catalyst with higher leaching property occurs in solution. Leached ferrous or ferric ions undergo conventional Fenton reaction cycles in the solution itself and form radicals. These radicals are responsible for the degradation of organic pollutants. Leaching of iron is the key factor in the enhanced removal of contaminants in the presence of a pyrite Fenton system. Choi *et al.*[93] reported that continuous dissolution of iron from pyrite is responsible for the degradation of pyrene. A similar result has been observed for the degradation of diclofenac.[91] A higher amount of ferrous ions leaching from natural pyrite during a Fenton reaction was observed by Wu *et al.*[94] These ferrous ions undergo conventional Fenton reactions and the oxidative species produced by the homogeneous Fenton reaction is the main reason for the degradation of azo dyes.

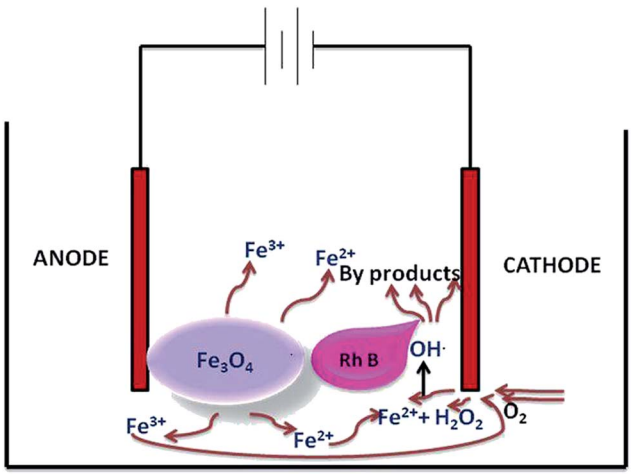

Fig. 6 Dye degradation mechanism of magnetite in electro Fenton process. Figure taken from ref. 80.

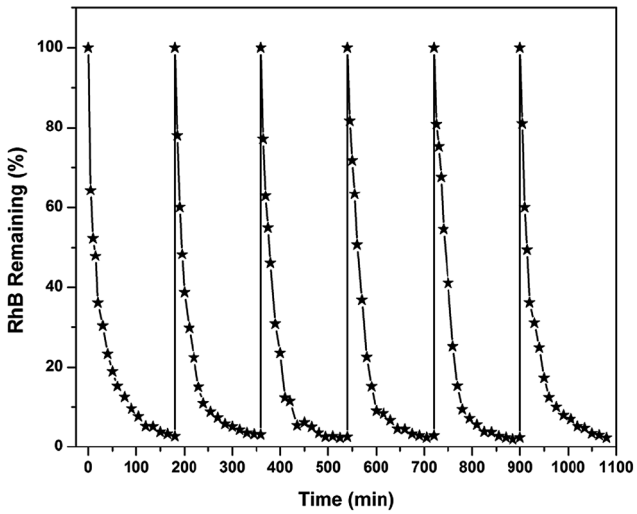

Fig. 7 Reusable nature of magnetite for the electro Fenton oxidation of rhodamine B. Figure taken from ref. 80.

Iron oxides exhibit multiple pollutant degradation mechanisms. Mineralization of organic compounds in the presence of goethite takes place in two ways.[52] In the first stage, degradation of pollutants occurs *via* hydroxyl radicals produced by reactions at the goethite surface. In the second stage of oxidation, degradation of pollutants occurs *via* hydroxyl radicals generated from classical Fenton reactions. Decomposition of hydrogen peroxide itself may take place in two ways, namely (1) a surface oxygen vacancies mechanism and (2) radical reactions.[94] In the first decomposition mechanism, oxygen vacancies on the surface of the catalyst cause the reduction of hydrogen peroxide to lattice oxygen which will then be desorbed as oxygen.[246,247] Sun and Lemley[72] observed a higher ratio of hydrogen peroxide consumed to the pollutant degraded. From this ratio, the authors concluded that the degradation of a pollutant occurs mainly *via* surface decomposition of hydrogen peroxide and subsequent production of perhydroxyl radicals, superoxide radicals and hydroperoxide anions in addition to hydroxyl radicals. The radical reaction mechanism of hydrogen peroxide decomposition is predominantly based on Fenton reactions.

Fenton oxidation of a pollutant in the presence of magnetite occurs mainly *via* hydroxyl radicals produced on its surface. This is mainly due to the fact that reversible oxidation and reduction of Fe species within the same structure is possible in magnetite and this possibility is mainly due to the existence of ferrous and ferric ions in octahedral sites of the magnetite structure.[74] However, the application of electricity to the Fenton process changed the pollutant degradation mechanism of magnetite from a surface reaction to a Fenton reaction in solution.[80] The presence of higher electrode potential increased the leaching of metals from magnetite. The leached iron species are attracted towards the cathode, react with electrolytically generated hydrogen peroxide at the cathode and form hydroxyl radicals, as shown in Fig. 6.

Stability of catalyst

The stability or reusability of the catalyst is one of the major advantages of heterogeneous Fenton processes over homogeneous Fenton processes. In the case of a homogeneous Fenton process, the iron content in solution decreased with reaction time due to sludge formation. As the rest of the ferrous ions are homogeneously dissolved in water, it is very difficult to separate them. However, in the case of a heterogeneous Fenton process, all the catalysts are solid and are very easy to separate from solution.

As well as its activity, the stability of a catalyst is very important when considering its industrial application. Reusability of the catalyst reduces the cost of wastewater treatment. Most heterogeneous catalysts used in the Fenton reaction are highly stable. For example, magnetite displayed higher stability even after five cycles. The reusable nature of magnetite during electro Fenton oxidation of rhodamine B is shown in Fig. 7.

Issues related to heterogeneous Fenton catalysts and perspectives

Although heterogeneous Fenton catalysts have several advantages such as reusability, higher activity in wide pH ranges, *etc.* there are some issues which delay the application of heterogeneous Fenton catalysts. One main problem is higher leaching of iron species from the catalyst, as discussed in an earlier section. This higher leaching of iron species from catalysts adversely affects their reusability. Another problem is deactivation of heterogeneous catalysts. The main causes of the deactivation of heterogeneous catalysts are poisoning, fouling or coking, thermal degradation (sintering, evaporation), mechanical damage and corrosion/leaching by the reaction mixture.[248–250] Poisoning is deactivation of heterogeneous catalysts by extensive adsorption of impurities present in the feed stream.[248] Fouling or coking is physical (mechanical) deposition of species from a fluid phase onto the catalyst surface, which results in a loss of activity due to blockage of sites and/or pores.[250] Thermal degradation is a physical process leading to catalyst deactivation because of sintering, chemical transformations, evaporation, *etc.*[249] Among these, sintering occurs mainly *via* structural modification of catalysts. Sintering may be either loss of catalytic surface area due to crystallite growth in the catalytic phase, or loss of catalytic support area due to collapse of the support and of catalytic surface area due to the collapse of pores in crystallites of the active phase.[250]

Deactivation of heterogeneous Fenton catalysts has been observed by various authors. For example, Fe-MSP[150] is not stable, even though it displays low leaching properties. This reduction in the catalytic activity of the catalyst is mainly due to poisoning of active sites by sorption of pollutants and the difficulty of removing these adsorbed materials from active catalytic sites during washing and drying processes.[136,189]

The application of heterogeneous Fenton processes on an industrial scale has not yet been implemented. This is mainly due to deactivation of catalysts during the reactions. Therefore, effort aimed at the development of new catalysts which exhibit high stability with low deactivation and leaching will constitute a major factor. Purification of deactivated catalysts, especially the support materials, is also very important. Another challenge in the future is to increase the surface area of catalysts and enhance the activity of catalysts by doping of metal ions in Fenton catalysts with low leaching properties.

Conclusions

Heterogeneous Fenton processes possess the ability to degrade persistent organic pollutants in wastewater. Research is more focused on improvement in the catalytic activity and stability of various catalysts. Heterogeneous Fenton catalysts exhibited higher catalytic activity over a wide range of reaction pH and an increased kinetic rate compared to homogeneous Fenton catalysts. Solid catalysts such as iron minerals, soils, waste materials containing iron species, iron- and iron oxide-loaded materials, *etc.*, possess greater ability to degrade pollutants in the presence of hydrogen peroxide. Research focuses more on enhancing the Fenton activity of catalysts by increasing their surface area and doping with other metals. Based on their leaching properties, catalysts exhibited different stability and pollutant degradation mechanisms. Most heterogeneous catalysts displayed less leaching property. In these cases, Fenton reactions occurred on the surface of the catalyst. Some catalysts exhibited the leaching of a significant amount of iron with pollutant degradation dominated by homogeneous Fenton reactions in the presence of leached iron species. Heterogeneous Fenton-like catalysts also display high catalytic activity for the degradation of pollutants. Deactivation is the main drawback of these catalysts, which reduces the reaction rate and reusability of heterogeneous catalysts. The Fenton process with catalysts which display higher catalytic activity and stability is a promising technology in the field of wastewater treatment.

References

1 E. Brillas, I. Sires and M. A. Oturan, *Chem. Rev.*, 2009, **109**, 6570–6631.
2 M. A. Oturan, *J. Appl. Electrochem.*, 2000, **30**, 475–482.
3 J. J. Pignatello, E. Oliveros and A. Mackay, *Crit. Rev. Environ. Sci. Technol.*, 2006, **36**, 1–84.
4 E. Neyens and J. Baeyens, *J. Hazard. Mater.*, 2003, **B98**, 33–50.
5 P. V. Nidheesh, R. Gandhimathi and S. T. Ramesh, *Environ. Sci. Pollut. Res.*, 2013, **20**, 2099–2132.
6 P. V. Nidheesh and R. Gandhimathi, *Desalination*, 2012, **299**, 1–15.
7 W. S. Chen and S. Z. Lin, *J. Hazard. Mater.*, 2009, **168**, 1562–1568.
8 M. Muruganandham and M. Swaminathan, *Dyes Pigm.*, 2004, **63**, 315–321.
9 P. R. Gogate and A. B. Pandit, *Adv. Environ. Res.*, 2004, **8**, 501–551.
10 P. R. Gogate and A. B. Pandit, *Adv. Environ. Res.*, 2004, **8**, 553–597.

11 V. Kavitha and K. Palanivelu, *Chemosphere*, 2004, **55**, 1235–1243.
12 A. Ž. Gotvajn and J. Zagorc-Končan, *Acta Chim. Slov.*, 2005, **52**, 131–137.
13 P. Bautista, A. F. Mohedano, M. A. Gilarranz, J. A. Casas and J. J. Rodriguez, *J. Hazard. Mater.*, 2007, **143**, 128–134.
14 M. A. Oturan, N. Oturan, C. Lahitte and S. Trevin, *Electroanal. Chem.*, 2001, **507**, 96–102.
15 P. V. Nidheesh and R. Gandhimathi, *Clean: Soil, Air, Water*, 2014, **42**, 779–784.
16 M. A. Oturan, M. C. Edelahi, N. Oturan, K. El kacemi and J.-J. Aaron, *Appl. Catal., B*, 2010, **97**, 82–89.
17 A. Özcan, Y. Şahin and M. A. Oturan, *Chemosphere*, 2008, **73**, 737–744.
18 S. J. George, R. Gandhimathi, P. V. Nidheesh and S. T. Ramesh, *Environ. Eng. Sci.*, 2013, **30**, 750–756.
19 P. V. Nidheesh, R. Gandhimathi and N. S. Sanjini, *Sep. Purif. Technol.*, 2014, **132**, 568–576.
20 I. Sirés, N. Oturan, M. A. Oturan, R. M. Rodríguez, J. A. Garrido and E. Brillas, *Electrochim. Acta*, 2007, **52**, 5493–5503.
21 P. V. Nidheesh and R. Gandhimathi, *J. Hazard., Toxic Radioact. Waste*, 2014, DOI: 10.1061/asce,hz.2153–5515.0000254.
22 M. Diagne, N. Oturan and M. A. Oturan, *Chemosphere*, 2007, **66**, 841–848.
23 S. J. George, R. Gandhimathi, P. V. Nidheesh and S. T. Ramesh, *Clean: Soil, Air, Water*, 2014, **42**, 1–11.
24 P. V. Nidheesh and R. Gandhimathi, *Desalin. Water Treat.*, 2014, DOI: 10.1080/19443994.2014.913266.
25 M. M. Ghoneim, H. S. El-Desoky and N. M. Zidan, *Desalination*, 2011, **274**, 22–30.
26 B. Gözmen, M. A. Oturan, N. Oturan and O. Erbatur, *Environ. Sci. Technol.*, 2003, **37**, 3716–3723.
27 P. V. Nidheesh and R. Gandhimathi, *Desalin. Water Treat.*, 2014, **52**, 1872–1877.
28 H. Kusic, N. Koprivanac and L. Srsan, *J. Photochem. Photobiol., A*, 2006, **181**, 195–202.
29 Y. G. Adewuyi, *Environ. Sci. Technol.*, 2005, **39**, 3409–3420.
30 C. Özdemir, M. K. Öden, S. Sahinkaya and E. Kalipci, *Clean: Soil, Air, Water*, 2011, **39**, 60–67.
31 T. T. H. Pham, S. K. Brar, R. D. Tyagi and R. Y. Surampalli, *Ultrason. Sonochem.*, 2010, **17**, 38–45.
32 S. Wang, *Dyes Pigm.*, 2008, **76**, 714–720.
33 H. S. El-Desoky, M. M. Ghoneim, R. El-Sheikh and N. M. Zidan, *J. Hazard. Mater.*, 2010, **175**, 858–865.
34 X. Zhang, Y. Chen, N. Zhao, H. Liuac and Y. Wei, *RSC Adv.*, 2014, **4**, 21575–21583.
35 *Advanced Oxidation Processes for Water and Wastewater Treatment*, ed. S. Parsons, IWA Publishing, London, 2004.
36 W. Huang, M. Brigante, F. Wu, K. Hanna and G. Mailhot, *Environ. Sci. Pollut. Res.*, 2013, **20**, 39–50.
37 H. Liu, Y. Wang, Y. Ma, Y. Wei and G. Pan, *Chemosphere*, 2010, **79**, 802–806.
38 Y. Wang, Y. Zhao, Y. Ma, H. Liu and Y. Wei, *J. Mol. Catal. A: Chem.*, 2010, **325**, 79–83.
39 R. M. Cornell and U. Schwertmann, *The Iron Oxides*, WILEY-VCH, New York, 2nd edn, 2003.
40 Y. Wu, R. Chen, H. Liu, Y. Wei and D. Wu, *React. Kinet., Mech. Catal.*, 2013, **110**, 87–99.
41 J. C. Barreiro, M. D. Capelato, L. Martin-Neto and H. C. B. Hansen, *Water Res.*, 2007, **41**, 55–62.
42 C. B. Carter and M. G. Norton, *Ceramic Materials: Science and Engineering*, Springer, 2007.
43 S. Jauhar, S. Singhal and M. Dhiman, *Appl. Catal., A*, 2014, **486**, 210–218.
44 S.-Q. Liu, L.-R. Feng, N. Xu, Z.-G. Chen and X.-M. Wang, *Chem. Eng. J.*, 2012, **203**, 432–439.
45 T. Soltani and M. H. Entezari, *Chem. Eng. J.*, 2014, **251**, 207–216.
46 B. Sahoo, S. K. Sahu, S. Nayak, D. Dhara and P. Pramanik, *Catal. Sci. Technol.*, 2012, **2**, 1367–1374.
47 S. Jauhar and S. Singhal, *Ceram. Int.*, 2014, **40**, 11845–11855.
48 C. Singh, A. Goyal and S. Singhal, *Nanoscale*, 2014, **6**, 7959–7970.
49 Wikipedia, http://en.wikipedia.org/wiki/Goethite, accessed on 3.12.2014.
50 G. B. Ortiz de la Plata, O. M. Alfano and A. E. Cassano, *Chem. Eng. J.*, 2008, **137**, 396–410.
51 M. Muruganandham, J.-S. Yang and J. J. Wu, *Ind. Eng. Chem. Res.*, 2007, **46**, 691–698.
52 T. R. Gordon and A. L. Marsh, *Catal. Lett.*, 2009, **132**, 349–354.
53 G. B. Ortiz de la Plata, O. M. Alfano and A. E. Cassano, *Appl. Catal., B*, 2010, **95**, 1–13.
54 G. B. Ortiz de la Plata, O. M. Alfano and A. E. Cassano, *Appl. Catal., B*, 2010, **95**, 14–25.
55 N. Dulova, M. Trapido and A. Dulov, *Environ. Technol.*, 2011, **32**, 439–446.
56 http://www.minerals.net/mineral/schorl.aspx, accessed on 3.12.2014.
57 Wikipedia, http://en.wikipedia.org/wiki/Tourmaline, accessed on 12.11.2014.
58 F. Yavuza, A. H. Gültekin and M. C. Karakaya, *Comput. Geosci.*, 2002, **28**, 1017–1036.
59 K. Shigenobu, T. Matsumura, T. Nakamura, H. Ishii and Y. Nishi, in *Proceedings First International Symposium on Environmentally Conscious Design and Inverse Manufacturing*, Tokyo, Japan, 1-3 Feb, 1999, pp. 912–915.
60 H.-Y. Xu, M. Prasad and Y. Liu, *J. Hazard. Mater.*, 2009, **165**, 1186–1192.
61 H. Y. Xu, M. Prasad, X. L. He, L. W. Shan and S. Y. Qi, *Sci. China, Ser. E: Technol. Sci.*, 2009, **52**, 3054–3060.
62 H. Y. Xu, M. Prasad, S. Y. Qi and Y. Li, *Sci. China: Technol. Sci.*, 2010, **53**, 3014–3019.
63 Wikipedia, http://en.wikipedia.org/wiki/Hematite, Contents accessed on 3.12.2014.
64 F. V. F. Araujo, L. Yokoyama, L. A. C. Teixeira and J. C. Campos, *Braz. J. Chem. Eng.*, 2011, **28**, 605–616.
65 Z. Cao, M. Qin, B. Jia, Y. Gu, P. Chen, A. A. Volinsky and X. Qu, *Ceram. Int.*, 2015, **41**, 2806–2812.

66 A. C. Silva, D. Q. L. Oliveira, L. C. A. Oliveira, A. S. Anastácio, T. C. Ramalho, J. H. Lopes, H. W. P. Carvalho and C. E. Rodriguez Torres, *Appl. Catal., A*, 2009, **357**, 79–84.
67 H. S. Oliveira, L. D. Almeida, V. A. A. de Freitas, F. C. C. Moura, P. P. Souza and L. C. A. Oliveira, *Catal. Today*, 2015, **240**, 176–181.
68 N. Ameta, J. Sharma, S. Sharma, S. Kumar and P. B. Punjabi, *Indian J. Chem.*, 2012, **51**, 943–948.
69 J. Shi, Z. Ai and L. Zhang, *Water Res.*, 2014, **59**, 145–153.
70 L. Guo, F. Chen, X. Fan, W. Cai and J. Zhang, *Appl. Catal., B*, 2010, **96**, 162–168.
71 G. K. Pradhan, N. Sahu and K. M. Parida, *RSC Adv.*, 2013, **3**, 7912–7920.
72 S.-P. Sun and A. T. Lemley, *J. Mol. Catal. A: Chem.*, 2011, **349**, 71–79.
73 R. J. Harrison, R. E. Dunnin-Borkowski and A. Putnis, *Proc. Natl. Acad. Sci. U. S. A.*, 2002, **99**, 16556–16561.
74 R. C. C. Costa, M. F. F. Lelis, L. C. A. Oliveira, J. D. Fabris, J. D. Ardisson, R. R. V. A. Rios, C. N. Silva and R. M. Lago, *J. Hazard. Mater.*, 2006, **129**, 171–178.
75 S. R. Pouran, A. R. Abdul Aziz, W. M. A. W. Daud and S. Shamshirband, *Measurement*, 2015, **59**, 314–328.
76 Z. X. Sun, F. W. Su, W. Forsling and P. O. Samskog, *J. Colloid Interface Sci.*, 1998, **197**, 151–159.
77 X. Hu, B. Liu, Y. Deng, H. Chen, S. Luo, C. Sun, P. Yang and S. Yang, *Appl. Catal., B*, 2011, **107**, 274–283.
78 L. M. Pastrana-Martínez, N. Pereira, R. Lima, J. L. Faria, H. T. Gomes and A. M. T. Silva, *Chem. Eng. J.*, 2015, **261**, 45–52.
79 J. He, X. Yang, B. Men, Z. Bi, Y. Pu and D. Wang, *Chem. Eng. J.*, 2014, **258**, 433–441.
80 P. V. Nidheesh, R. Gandhimathi, S. Velmathi and N. S. Sanjini, *RSC Adv.*, 2014, **4**, 5698–5708.
81 S. Xavier, R. Gandhimathi, P. V. Nidheesh and S. T. Ramesh, *Desalin. Water Treat.*, 2015, **53**, 109–118.
82 I. L. Júnior, J. M. M. Millet, M. Aouine and M. do Carmo Rangel, *Appl. Catal., A*, 2005, **283**, 91–98.
83 X. Liang, S. Zhu, Y. Zhong, J. Zhu, P. Yuan, H. He and J. Zhang, *Appl. Catal., B*, 2010, **97**, 151–159.
84 Y. Zhong, X. Liang, Y. Zhong, J. Zhu, S. Zhu, P. Yuan, H. He and J. Zhang, *Water Res.*, 2012, **46**, 4633–4644.
85 M. Luo, S. Yuan, M. Tong, P. Liao, W. Xie and X. Xu, *Water Res.*, 2014, **48**, 190–199.
86 D. Q. L. Oliveira, L. C. A. Oliveira, E. Murad, J. D. Fabris, A. C. Silva and L. M. de Menezes, *Hyperfine Interact.*, 2010, **195**, 27–34.
87 Y. Zhong, X. Liang, Z. He, W. Tan, J. Zhu, P. Yuan, R. Zhu and H. He, *Appl. Catal., B*, 2014, **150–151**, 612–618.
88 Wikipedia, http://en.wikipedia.org/wiki/Pyrite, accessed on 3.12.2014.
89 C. A. Cohn, S. Mueller, E. Wimmer, N. Leifer, S. Greenbaum, D. R. Strongin and M. A. A. Schoonen, *Geochem. Trans.*, 2006, **7**, 3.
90 H. Che, S. Bae and W. Lee, *J. Hazard. Mater.*, 2011, **185**, 1355–1361.
91 S. Bae, D. Kim and W. Lee, *Appl. Catal., B*, 2013, **134–135**, 93–102.
92 Y. Zhang, K. Zhang, C. Dai, X. Zhou and H. Si, *Chem. Eng. J.*, 2014, **244**, 438–445.
93 K. Choi, S. Bae and W. Lee, *Chem. Eng. J.*, 2014, **249**, 34–41.
94 D. Wu, Y. Feng and L. Ma, *Water, Air, Soil Pollut.*, 2013, **224**, 1407.
95 W. Wang, Y. Qu, B. Yang, X. Liu and W. Su, *Chemosphere*, 2012, **86**, 376–382.
96 N. Deng, F. Luo, F. Wu, M. Xiao and X. Wu, *Water Res.*, 2000, **34**, 2408–2411.
97 R. A. Crane and T. B. Scott, *J. Hazard. Mater.*, 2012, **211–212**, 112–125.
98 Y.-P. Sun, X.-Q. Li, J. Cao, W.-X. Zhang and H. Paul Wang, *Adv. Colloid Interface Sci.*, 2006, **120**, 47–56.
99 F. Fu, Q. Wang and B. Tang, *J. Hazard. Mater.*, 2010, **174**, 17–22.
100 A. Naldoni, A. Schiboula, C. L. Bianchi and D. H. Bremner, *Water, Air, Soil Pollut.*, 2011, **215**, 487–495.
101 Z. W. Min, T.-H. Kim, J.-H. Shin, S.-M. Lee and J.-E. Kim, *J. Korean Soc. Appl. Biol. Chem.*, 2009, **52**, 681–687.
102 M. R. Taha and A. H. Ibrahim, *J. Water Process Eng.*, 2014, **1**, 8–16.
103 B. Li and J. Zhu, *Chem. Eng. J.*, 2014, **255**, 225–232.
104 S. Zha, Y. Cheng, Y. Gao, Z. Chen, M. Megharaj and R. Naidu, *Chem. Eng. J.*, 2014, **255**, 141–148.
105 X. Q. Li and W. X. Zhang, *J. Phys. Chem. C*, 2007, **111**, 6939–6946.
106 X. Yin, W. Liu and J. Ni, *Chem. Eng. J.*, 2014, **248**, 89–97.
107 R.-F. Yu, H.-W. Chen, W.-P. Cheng, Y.-J. Lin and C.-L. Huang, *J. Taiwan Inst. Chem. Eng.*, 2014, **45**, 947–954.
108 S. Mohan and R. Gandhimathi, *J. Hazard. Mater.*, 2009, **169**, 351–359.
109 Wikipedia, http://en.wikipedia.org/wiki/Fly_ash, accessed on 18.11.2014.
110 S. Wang, *Environ. Sci. Technol.*, 2008, **42**, 7055–7063.
111 S.-H. Chen and D.-Y. Du, *J. Cent. South Univ.*, 2014, **21**, 1448–1452.
112 Y.-L. Song and J.-T. Li, *Ultrason. Sonochem.*, 2009, **16**, 440–444.
113 J.-T. Li, B. Bai and Y.-L. Song, *Indian J. Chem. Technol.*, 2010, **17**, 198–203.
114 D. S. Duc, *Asian J. Chem.*, 2013, **25**, 4083–4086.
115 A. Zhang, N. Wang, J. Zhou, P. Jiang and G. Liu, *J. Hazard. Mater.*, 2012, **201–202**, 68–73.
116 Y. Flores, R. Flores and A. A. Gallegos, *J. Mol. Catal. A: Chem.*, 2008, **281**, 184–191.
117 R. Mecozzi, L. Di Palma, D. Pilone and L. Cerboni, *J. Hazard. Mater.*, 2006, **B137**, 886–892.
118 C. C. Amorim, M. M. D. Leão, R. F. P. M. Moreira, J. D. Fabris and A. B. Henriques, *Chem. Eng. J.*, 2013, **224**, 59–66.
119 C. Patel Darshna and C. Rotliwala Yogesh, *J. Environ. Res. Dev.*, 2014, **8**, 983–986.
120 C. Yang, Y. Chen, P. Peng, C. Li, X. Chang and Y. Wu, *J. Hazard. Mater.*, 2009, **167**, 835–845.

121 M. Becelic-Tomin, B. Dalmacija, L. Rajic, D. Tomasevic, D. Kerkez, M. Watson and M. Prica, *Scientific World J.*, 2014, DOI: 10.1155/2014/234654.
122 R. C. Martins, L. R. Henriques and R. M. Quinta-Ferreira, *Chem. Eng. Sci.*, 2013, **100**, 225–233.
123 M. E. M. Ali, T. A. Gad-Allah and M. I. Badawy, *Appl. Water Sci.*, 2013, **3**, 263–270.
124 P. V. Nidheesh and R. Gandhimathi, *RSC Adv.*, 2014, **4**, 27946–27954.
125 W. Wang, M. Zhou, Q. Mao, J. Yue and X. Wang, *Catal. Commun.*, 2010, **11**, 937–941.
126 Y. Yao, Y. Cai, F. Lu, J. Qin, F. Wei, C. Xu and S. Wang, *Ind. Eng. Chem. Res.*, 2014, **53**, 17294–17302.
127 P. Shukla, S. Wang, H. Sun, H.-M. Ang and M. Tadé, *Chem. Eng. J.*, 2010, **164**, 255–260.
128 Y. Yao, J. Qin, Y. Cai, F. Wei, F. Lu and S. Wang, *Environ. Sci. Pollut. Res.*, 2014, **21**, 7296–7306.
129 Wikipedia, http://en.wikipedia.org/wiki/Activated_carbon, accessed on 18.11.2014.
130 M. F. R. Pereira, J. J. M. Órfão and J. L. Figueiredo, *Colloids Surf., A*, 2004, **241**, 165–171.
131 G. Sekaran, S. Karthikeyan, K. Ramani, B. Ravindran, A. Gnanamani and A. B. Mandal, *Environ. Chem. Lett.*, 2011, **9**, 499–504.
132 S. Karthikeyan, M. Ezhil Priya, R. Boopathy, M. Velan, A. B. Mandal and G. Sekaran, *Environ. Sci. Pollut. Res.*, 2012, **19**, 1828–1840.
133 G. Sekaran, S. Karthikeyan, R. Boopathy, P. Maharaja, V. K. Gupta and C. Anandan, *Environ. Sci. Pollut. Res.*, 2014, **21**, 1489–1502.
134 S. Karthikeyan, C. Judia Magthalin, A. B. Mandal and G. Sekaran, *RSC Adv.*, 2014, **4**, 19183–19195.
135 Y. Yao, L. Wang, L. Sun, S. Zhu, Z. Huang, Y. Mao, W. Lu and W. Chen, *Chem. Eng. Sci.*, 2013, **101**, 424–431.
136 T. D. Nguyen, N. H. Phan, M. H. Do and K. T. Ngo, *J. Hazard. Mater.*, 2011, **185**, 653–661.
137 Z. Cherkezova-Zheleva, D. Paneva, M. Tsvetkov, B. Kunev, M. Milanova, N. Petrov and I. Mitov, *Hyperfine Interact.*, 2014, **226**, 517–527.
138 C. Yang, D. Wang and Q. Tang, *J. Taiwan Inst. Chem. Eng.*, 2014, **45**, 2584–2589.
139 C. Zhang, L. Zhou, J. Yang, X. Yu, Y. Jiang and M. Zhou, *Environ. Sci. Pollut. Res.*, 2014, **21**, 8398–8405.
140 S. A. Messele, O. S. G. P. Soares, J. J. M. Órfão, C. Bengoa, F. Stüber, A. Fortuny, A. Fabregat and J. Font, *Catal. Today*, 2015, **240**, 73–79.
141 Y. Tu, Y. Xiong, C. Descorme, L. Kong and S. Tian, *J. Chem. Technol. Biotechnol.*, 2014, **89**, 544–551.
142 S.-J. Yuan and X.-H. Dai, *Appl. Catal., B*, 2014, **154–155**, 252–258.
143 V. Cleveland, J.-P. Bingham and E. Kan, *Sep. Purif. Technol.*, 2014, **133**, 388–395.
144 A. N. Soon and B. H. Hameed, *Desalination*, 2011, **269**, 1–16.
145 P. Ghosh, C. Kumar, A. N. Samanta and S. Ray, *J. Chem. Technol. Biotechnol.*, 2012, **87**, 914–923.
146 P. Bautista, A. F. Mohedano, J. A. Casas, J. A. Zazo and J. J. Rodriguez, *J. Chem. Technol. Biotechnol.*, 2011, **86**, 497–504.
147 Z. Li, J. Sheng, Y. Wang and Y. Xu, *J. Hazard. Mater.*, 2013, **254–255**, 18–25.
148 Y. Hu and S. Lu, *Int. J. Eng. Sci. Technol.*, 2010, **2**, 110–114.
149 X. Zhong, L. Xiang, S. Royer, S. Valange, J. Barrault and H. Zhang, *J. Chem. Technol. Biotechnol.*, 2011, **86**, 970–977.
150 A. R. Laiju, T. Sivasankar and P. V. Nidheesh, *Environ. Sci. Pollut. Res.*, 2014, **21**, 10900–10907.
151 N. K. Daud and B. H. Hameed, *J. Hazard. Mater.*, 2010, **176**, 938–944.
152 G. Ersöz, *Appl. Catal., B*, 2014, **147**, 353–358.
153 G. Tekin, G. Ersöz and S. Atalay, in *Digital Proceeding of THE ICOEST'2013*, Nevsehir, Turkey, June 18–21, 2013.
154 J. Wu, J. Zhao, F. Du and Z. Han, *J. Sustainable Dev.*, 2009, **2**, 214–220.
155 G. T. Chi, J. Churchley and K. D. Huddersman, *Int. J. Chem. Eng.*, 2013, DOI: 10.1155/2013/760915.
156 G. T. Chi and K. D. Huddersman, *J. Adv. Oxid. Technol.*, 2011, **14**, 235–243.
157 G. T. Chi, Z. K. Nagy and K. D. Huddersman, *Prog. React. Kinet. Mech.*, 2011, **36**, 189–214.
158 X. Zhao, Y. Dong, B. Cheng and W. Kang, *Int. J. Photoenergy*, 2013, DOI: 10.1155/2013/820165.
159 Z. Ding, Y. Dong and B. Li, *Int. J. Photoenergy*, 2012, DOI: 10.1155/2012/121239.
160 B. Li, Y. Dong, Z. Ding, Y. Xu and C. Zou, *Int. J. Photoenergy*, 2013, DOI: 10.1155/2013/169493.
161 B. Li, Y. Dong, M. Li and Z. Ding, *J. Mater. Sci.*, 2014, **49**, 7639–7647.
162 L. Wang, Y. Yao, Z. Zhang, L. Sun, W. Lu, W. Chen and H. Chen, *Chem. Eng. J.*, 2014, **251**, 348–354.
163 X. Zhong, S. Royer, H. Zhang, Q. Huang, L. Xiang, S. Valange and J. Barrault, *Sep. Purif. Technol.*, 2011, **80**, 163–171.
164 M. Wang, Z. Shu, L. Zhang, X. Fan, G. Tao, Y. Wang, L. Chen, M. Wu and J. Shi, *Dalton Trans.*, 2014, 9234–9241.
165 L. Machala, R. Zboril and A. Gedanken, *J. Phys. Chem. B*, 2007, **111**, 4003–4018.
166 A. E. Nogueira, I. A. Castro, A. S. Giroto and Z. M. Magriotis, *J. Catal.*, 2014, DOI: 10.1155/2014/712067.
167 A. C. Pradhan and K. M. Parida, *J. Mater. Chem.*, 2012, **22**, 7567–7579.
168 C. Zhao, Y. P. Huang, Y. F. Fang, L. R. Jiang, L. M. Liu and K. T. Lau, *Chin. Sci. Bull.*, 2008, **53**, 1497–1502.
169 Y. Chen, S. Jin, J. Liu, B. Zhao and T. Wang, *Inorg. Chim. Acta*, 2013, **406**, 37–43.
170 Z. Miao, S. Tao, Y. Wang, Y. Yu, C. Meng and Y. An, *Microporous Mesoporous Mater.*, 2013, **176**, 178–185.
171 P. P. Gan and S. F. Y. Li, *Chem. Eng. J.*, 2013, **229**, 351–363.
172 Wikipedia, http://en.wikipedia.org/wiki/Zeolite, accessed on 29.12.2014.
173 S. Navalon, M. Alvaro and H. Garcia, *Appl. Catal., B*, 2010, **99**, 1–26.
174 R. Gonzalez-Olmos, M. J. Martin, A. Georgi, F.-D. Kopinke, I. Oller and S. Malato, *Appl. Catal., B*, 2012, **125**, 51–58.

175 S. Fukuchi, R. Nishimoto, M. Fukushima and Q. Zhu, *Appl. Catal., B*, 2014, **147**, 411–419.
176 J. Zhang, F.-T. Hu, Q.-Q. Liu, X. Zhao and S.-Q. Liu, *React. Kinet., Mech. Catal.*, 2011, **103**, 299–310.
177 Y. Yan, S. Jiang, H. Zhang and X. Zhang, *Chem. Eng. J.*, 2015, **259**, 243–251.
178 Y.-Y. Zhang, C. He, V. K. Sharma, X.-Z. Li, S.-H. Tian and Y. Xiong, *J. Chem. Technol. Biotechnol.*, 2011, **86**, 1488–1494.
179 E. Bocos, M. Pazos and M. A. Sanromán, *J. Chem. Technol. Biotechnol.*, 2014, **89**, 1235–1242.
180 L. F. González-Bahamón, F. Mazille, L. N. Benítez and C. Pulgarín, *J. Photochem. Photobiol., A*, 2011, **217**, 201–206.
181 T. A. Vu, G. H. Le, C. D. Dao, L. Q. Dang, K. T. Nguyen, P. T. Dang, H. T. K. Tran, Q. T. Duong, T. V. Nguyen and G. D. Lee, *RSC Adv.*, 2014, **4**, 41185–41194.
182 M. D. Gidigasu, *Eng. Geol.*, 1972, **4**, 79–91.
183 B. Manu and Mahamood, *Int. J. Earth Sci. Eng.*, 2011, **4**, 1103–1110.
184 A. R. Khataee and S. G. Pakdehi, *J. Taiwan Inst. Chem. Eng.*, 2014, **45**, 2664–2672.
185 R. Karale, B. Manu and S. Shrihari, *Int. J. Sci. Eng. Res.*, 2013, **4**, 207–210.
186 H. Hassan and B. H. Hameed, *Int. J. Environ. Sci. Dev.*, 2011, **2**, 218–222.
187 Wikipedia, http://en.wikipedia.org/wiki/Clay_minerals, accessed on 10.12.2014.
188 H. Hassan and B. H. Hameed, *Chem. Eng. J.*, 2011, **171**, 912–918.
189 L. Djeffal, S. Abderrahmane, M. Benzina, M. Fourmentin, S. Siffert and S. Fourmentin, *Environ. Sci. Pollut. Res.*, 2014, **21**, 3331–3338.
190 J. Herney-Ramirez, M. A. Vicente and L. M. Madeira, *Appl. Catal., B*, 2010, **98**, 10–26.
191 R. A. Schoonheydt, T. Pinnavaia, G. Lagaly and N. Gangas, *Pure Appl. Chem.*, 1999, **71**, 2368–2371.
192 M. Hartmann, S. Kullmann and H. Keller, *J. Mater. Chem.*, 2010, **20**, 9002–9017.
193 A. Gil, S. A. Korili, R. Trujillano and M. A. Vicente, *Appl. Clay Sci.*, 2011, **53**, 97–105.
194 J. T. Kloprogge, L. V. Duong and R. L. Frost, *Environ. Geol.*, 2005, **47**, 967–981.
195 C. B. Molina, J. A. Casas, A. H. Pizarro and J. J. Rodriguez, in *Clay: Types, Properties and Uses*, ed. J. P. Humphrey and D. E. Boyd, Nova Science Publishers Inc., New York, 2011, pp. 435–474.
196 M. A. De León, M. Sergio and J. Bussi, *React. Kinet., Mech. Catal.*, 2013, **110**, 101–117.
197 J.-M. Tatibouët, E. Guélou and J. Fournier, *Top. Catal.*, 2005, **33**, 225–232.
198 Wikipedia, http://en.wikipedia.org/wiki/Bentonite, accessed on 18.11.2014.
199 R. Arora, K. Chanderia, P. B. Punjabi and V. K. Sharma, *J. Chem. Pharm. Res.*, 2010, **2**, 627–636.
200 C. Catrinescu, C. Teodosiu, M. Macoveanu, J. Miehe-Brendle and R. Le Dred, *Environ. Eng. Manage. J.*, 2002, **1**, 561–569.
201 Y. Li, Y. Jin and H. Li, *React. Kinet. Catal. Lett.*, 2005, **85**, 313–321.
202 Y.-P. Zhang, C.-G. Jia, R. Peng, F. Ma and G.-N. Ou, *J. Cent. South Univ.*, 2014, **21**, 310–316.
203 J. Feng, X. Hu and P. L. Yue, *Water Res.*, 2005, **39**, 89–96.
204 BYK, Technical Information B-RI 21, LAPONITE®: Performance Additives, http://www.byk.com/fileadmin/byk/additives/product_groups/rheology/former_rockwood_additives/technical_brochures/BYK_B-RI21_LAPONITE_EN.pdf, accessed on 18.11.2014.
205 N. Willenbacher, *J. Colloid Interface Sci.*, 1996, **182**, 501–510.
206 A. Shahin and Y. M. Joshi, *Phys. Rev. Lett.*, 2011, **106**, DOI: 10.1103/physrevlett.106.038302.
207 J. Feng, X. Hu, P. L. Yue, H. Y. Zhu and G. Q. Lu, *Chem. Eng. Sci.*, 2003, **58**, 679–685.
208 J. Feng, X. Hu, P. L. Yue, H. Y. Zhu and G. Q. Lu, *Water Res.*, 2003, **37**, 3776–3784.
209 O. S. N. Sum, J. Feng, X. Hu and P. L. Yue, *Top. Catal.*, 2005, **33**, 233–242.
210 B. Iurascu, I. Siminiceanu, D. Vione, M. A. Vicente and A. Gil, *Water Res.*, 2009, **43**, 1313–1322.
211 Wikipedia, http://en.wikipedia.org/wiki/Montmorillonite, accessed on 10.12.2014.
212 O. B. Ayodele, J. K. Lim and B. H. Hameed, *Appl. Catal., A*, 2012, **413–414**, 301–309.
213 S. Zhang, S. Liang, X. Wang, J. Long, Z. Li and L. Wu, *Catal. Today*, 2011, **175**, 362–369.
214 M. A. De León, M. Sergio, J. Bussi, G. B. Ortiz de la Plata, A. E. Cassano and O. M. Alfano, *Environ. Sci. Pollut. Res.*, 2015, **22**, 864–869.
215 I. Muthuvel, B. Krishnakumar and M. Swaminathan, *Indian J. Chem., Sect. A: Inorg., Bio-inorg., Phys., Theor. Anal. Chem.*, 2012, **51**, 800–806.
216 A. C. Pradhan, G. Bishwa Bidita Varadwaj and K. M. Parida, *Dalton Trans.*, 2013, 15139–15149.
217 S. Kouraichi, M. El-Hadi Samar, M. Abbessi, H. Boudouh and A. Balaska, *Catal. Sci. Technol.*, 2015, **5**, 1052–1064.
218 Wikipedia, http://en.wikipedia.org/wiki/Saponite, accessed on 10.12.2014.
219 J. Herney Ramirez, C. A. Costa, L. M. Madeira, G. Mata, M. A. Vicente, M. L. Rojas-Cervantes, A. J. López-Peinado and R. M. Martín-Aranda, *Appl. Catal., B*, 2007, **71**, 44–56.
220 Wikipedia, http://en.wikipedia.org/wiki/Sepiolite, accessed on 10.12.2014.
221 J. Santaren, J. Sanz and E. Ruiz-Hitzky, *Clays Clay Miner.*, 1990, **38**, 63–68.
222 E. Sabah and M. Majdan, *J. Food Eng.*, 2009, **91**, 423–427.
223 O. Iglesias, M. A. Fernández de Dios, M. Pazos and M. A. Sanromán, *Environ. Sci. Pollut. Res.*, 2013, **20**, 5983–5993.
224 Y. Gao, H. Gan, G. Zhang and Y. Guo, *Chem. Eng. J.*, 2013, **217**, 221–230.
225 C. Su, W. Li, X. Liu, X. Huang and X. Yu, *Front. Environ. Sci. Eng.*, 2014, DOI: 10.1007/s11783-014-0729-y.
226 Wikipedia, http://en.wikipedia.org/wiki/Vermiculite, accessed on 10.12.2014.

227 S. C. Tjong, Y. Z. Meng and A. S. Hay, *Chem. Mater.*, 2002, **14**, 44–51.
228 F. J. del Rey-Perez-Caballero and G. Poncelet, *Microporous Mesoporous Mater.*, 2000, **37**, 313–327.
229 A. D. Purceno, A. P. C. Teixeira, A. B. Souza, J. D. Ardisson, J. P. de Mesquita and R. M. Lago, *Appl. Clay Sci.*, 2012, **69**, 87–92.
230 Q. Chen, P. Wu, Z. Dang, N. Zhu, P. Li, J. Wu and X. Wang, *Sep. Purif. Technol.*, 2010, **71**, 315–323.
231 W. A. Deer, R. A. Howie and J. Zussman, *An introduction to the reock-forming minerals*, Harlow: Longman, 2nd edn, 1992.
232 K. G. Bhattacharyya and S. S. Gupta, *Adv. Colloid Interface Sci.*, 2008, **40**, 114–131.
233 Wikipedia, http://en.wikipedia.org/wiki/Kaolinite, accessed on 10.12.2014.
234 O. B. Ayodele and B. H. Hameed, *Appl. Clay Sci.*, 2013, **83–84**, 171–181.
235 O. B. Ayodele, *Appl. Clay Sci.*, 2013, **72**, 74–83.
236 X. Liu, F. Wang, Z. Chen, M. Megharaj and R. Naidu, *Environ. Sci. Pollut. Res.*, 2014, **21**, 1936–1943.
237 S. Guo, G. Zhang and J. Wang, *J. Colloid Interface Sci.*, 2014, **433**, 1–8.
238 A. D. Bokare and W. Choi, *J. Hazard. Mater.*, 2014, **275**, 121–135.
239 S. K. Ling, S. Wang and Y. Peng, *J. Hazard. Mater.*, 2010, **178**, 385–389.
240 S. Kalal, N. P. S. Chauhan, N. Ameta, R. Ameta, S. Kumar and P. B. Punjabi, *Korean J. Chem. Eng.*, 2014, **31**, 2183–2191.
241 A. Angı, D. Sanlı, C. Erkey and Ö. Birer, *Ultrason. Sonochem.*, 2014, **21**, 854–859.
242 B. K. Ghosh, S. Hazra, B. Naik and N. N. Ghosh, *Powder Technol.*, 2015, **269**, 371–378.
243 A. C. Pradhan, B. Nanda, K. M. Parida and M. Das, *Dalton Trans.*, 2013, 558–566.
244 K. Chanderia, S. Kalal, J. Sharma, N. Ameta and P. B. Punjabi, *Indian J. Chem., Sect. A: Inorg., Bio-inorg., Phys., Theor. Anal. Chem.*, 2013, **52**, 1416–1420.
245 M. A. F. de Dios, E. Rosales, M. Fernández-Fernández, M. Pazos and M. Á. Sanromán, *J. Chem. Technol. Biotechnol.*, 2014, DOI: 10.1002/jctb.4446.
246 A. Georgi, A. Schierz, U. Trommler, C. P. Horwitz, T. J. Collins and F. D. Kopinke, *Appl. Catal., B*, 2007, **72**, 26–36.
247 Y. N. Lee, R. M. Lago, J. L. G. Fierro and J. González, *Appl. Catal., A*, 2001, **215**, 245–256.
248 P. Forzatti and L. Lietti, *Catal. Today*, 1999, **52**, 165–181.
249 J. A. Moulijn, A. E. van Diepen and F. Kapteijn, *Appl. Catal., A*, 2001, **212**, 3–16.
250 C. H. Bartholomew, *Appl. Catal., A*, 2001, **212**, 17–60.